VTT PUBLICATIONS 467

Transport Barrier and Current Profile Studies on the JET Tokamak

Tuomas Tala

VTT Processes

Dissertation for the degree of Doctor of Science in Technology
to be presented with due permission for public examination and debate
in Auditorium F1 at Helsinki University of Technology (Espoo, Finland)
on the 7th of June, 2002, at 12 o'clock noon.

ISBN 951–38–5988–6 (soft back ed.)
ISSN 1235–0621 (soft back ed.)

ISBN 951–38–5989–4 (URL: http://www.inf.vtt.fi/pdf/)
ISSN 1455–0849 (URL: http://www.inf.vtt.fi/pdf/)

JULKAISIJA – UTGIVARE – PUBLISHER

VTT, Vuorimiehentie 5, PL 2000, 02044 VTT
puh. vaihde (09) 4561, faksi (09) 456 4374

VTT, Bergsmansvägen 5, PB 2000, 02044 VTT
tel. växel (09) 4561, fax (09) 456 4374

VTT Technical Research Centre of Finland, Vuorimiehentie 5, P.O.Box 2000, FIN–02044 VTT, Finland
phone internat. + 358 9 4561, fax + 358 9 456 4374

VTT Prosessit, Otakaari 3 A, PL 1404, 02044 VTT
puh. vaihde (09) 4561, faksi (09) 456 6390

VTT Processer, Otsvängen 3 A, PB 1404, 02044 VTT
tel. växel (09) 4561, fax (09) 456 6390

VTT Processes, Otakaari 3 A, P.O.Box 1404, FIN–02044 VTT, Finland
phone internat. + 358 9 4561, fax + 358 9 456 6390

Technical editing Leena Ukskoski

Otamedia Oy, Espoo 2002

Tala, Tuomas. Transport Barrier and Current Profile Studies on the JET Tokamak. Espoo 2002. VTT Publications 467. 71 p. + app. 95 p.

Keywords nuclear fusion, JET tokamak, plasma transport, heat transport, internal transport barriers, current density, modelling, transport models, flow shear, magnetic shear

Abstract

One of the crucial problems in fusion research is the understanding of heat and particle transport in plasmas relevant for energy production. The neo-classical theory of tokamak transport is well-established, but it cannot explain experimental results. Instead, the micro-turbulence driven anomalous transport has been found to be dominant in present tokamak experiments.

There are several mechanisms that can locally suppress micro-turbulence and re- duce significantly the anomalous transport. These regions of reduced transport are called transport barriers. The presence of Internal Transport Barriers (ITBs) is one of the bases in 'Advanced Tokamak Scenarios'. One of the principal goals in the 'Advanced Tokamak Scenarios' is to improve the fusion power density and con- finement with internal transport barriers by controlling the current density profile and maximising the bootstrap current – and ultimately rendering the tokamak compatible with continuous operation.

This thesis reports on studies and modelling of internal transport barriers and current density profiles in the Joint European Torus (JET) tokamak with a fluid transport code. Explanations for the following open questions are sought: what are the mechanisms that govern the formation and dynamics of the ITBs in JET and secondly, how can the current density profile be modified and further, how does it affect ITBs and plasma performance?

On the basis of the empirical study at the ITB transition, the $\omega_{E\times B}$ flow shear and magnetic shear appear as strong candidates in determining the onset time, the radial location and the dynamics of the ITBs in JET. This ITB threshold condition, employed in the semi-empirical Bohm/GyroBohm transport model, has been found to be in good agreement with experimental results in predictive transport simulations. On the other hand, the simulation results from the predictive transport modelling with a theory-based quasi-linear fluid transport model strongly emphasise the importance of the density gradient in the ITB formation.

According to the current density modelling studies, lower hybrid and electron cyclotron current drive are the most versatile current drive methods in terms of the produced q-profile in the preheating phase in JET. With lower hybrid preheating, a core current hole has been found and a physics-based explanation, confirmed by the transport modelling, is given. The predictive transport simulations indicate that application of lower hybrid current drive during the high performance phase can enhance the fusion performance significantly by increasing the ITB radius.

Preface

The work reported in this thesis has been done at the Joint European Torus (JET) in Oxford, the United Kingdom, at VTT (Technical Research Centre of Finland) and at Helsinki University of Technology over a period of three and a half years from summer 1998 until spring 2002. The work has been carried out under the Euratom-TEKES Association Agreement and is a part of the Finnish and European fusion research programs.

I wish to express my deep gratitude to my instructor at JET, Dr. Vassili Parail for his continuous and thorough guidance and encouragement through the thesis. I also want acknowledge Dr. Clive Challis, Dr. Alain Becoulet and Dr. Franz Söldner for many valuable discussions and ideas during my stays at JET.

I am deeply indebted to my instructor at VTT, Dr. Jukka Heikkinen for his continuous guidance and interest in my work and for giving many useful comments through the thesis as well as reading carefully the manuscript. I would also like to acknowledge Dr. Seppo Karttunen for giving me the opportunity to work at JET for two years and the rest of the time at VTT. I also want to thank my supervisor, Prof. Rainer Salomaa, who gave me the first opportunity to work in the field of nuclear fusion.

My special thanks belong to my friends, colleagues and personnel at JET, VTT and Helsinki University of Technology for making my work over these years as pleasurable as it has been.

Financial support from the Fortum Foundation and Euratom is gratefully acknowledged.

I also want to thank my parents for their continuous interest and encouragement during the course of my studies. A large part of the work was carried out within time which would otherwise been spent with my dear wife Satu. I want to express my deep gratitude to her for being there all these years and you will deserve a huge hug right after the dissertation. And last but not least, major thanks to Miika, our dear son, for keeping my thoughts often enough outside the thesis.

Espoo, May 7, 2002

Tuomas Tala

List of Publications

This paper is an introduction to and a review of the main results reported in the following publications (reprinted in the appendices of this thesis):

1. Tala T.J.J., Heikkinen J.A., Parail V.V., Baranov Yu.F. and Karttunen S.J., "ITB formation in terms of $\omega_{E\times B}$ flow shear and magnetic shear s on JET", Plasma Phys. Control. Fusion **43** (2001) 507–523.

2. Tala T.J.J., Parail V.V., Becoulet A., Corrigan G., Heading D.J., Mantsinen M.J., Strand P.I. and contributors to the EFDA-JET workprogramme, "Comparison of theory-based and semi-empirical transport modelling in JET plasmas with ITBs", Plasma Phys. Control. Fusion **44** (2002) in press.

3. Tala T.J.J., Parail V.V., Becoulet A., Challis C.D., Corrigan G., Hawkes N.C., Heading D.J., Mantsinen M.J., Nowak S. and contributors to the EFDA-JET workprogramme, "Impact of different heating and current drive methods on the early q-profile evolution in JET", Plasma Phys. Control. Fusion **44** (2002) in press.

4. Hawkes N.C., Stratton B.C., Tala T.J.J., Challis C.D., Conway G., DeAngelis R., Giroud C., Hobirk J., Joffrin E., Lomas P., Lotte P., Mailloux J., Mazon D., Rachlew E., Reyes-Cortes S., Solano E. and Zastrow K.-D., "Observation of Zero Current Density in the Core of JET Discharges with Lower Hybrid Heating and Current Drive", Phys. Rev. Lett. **87** (2001) 115011-1–4.

5. Tala T.J.J., Söldner F.X., Parail V.V., Baranov Yu.F., Heikkinen J.A. and Karttunen S.J., "Modelling of optimized shear scenarios with LHCD for high performance experiments on JET", Nucl. Fusion **40** (2000) 1635–1649.

6. Heikkinen J.A., Tala T.J.J., Pättikangas T.J.H., Piliya A.D., Saveliev A.N. and Karttunen S.J., "Role of fast waves in the central deposition of lower hybrid power", Plasma Phys. Control. Fusion **41** (1999) 1231–1249.

The work carried out in this thesis is to resolve some of the many questions dealing with the incomplete picture of transport in tokamaks, in particular issues related to internal transport barriers. In Publication 1, the ITB formation mechanisms as

a function of local plasma parameters, i.e. the threshold where the confinement improves and transport reduces in the core region, are sought in plasmas of the JET tokamak. In addition, quantities that govern the further time evolution of the ITBs in JET are investigated.

After having found the empirical ITB formation threshold condition in JET, the threshold condition is implemented into the semi-empirical Bohm/GyroBohm transport model. The condition is then tested against a large database of the JET ITB discharges with JETTO transport code (Publication 1). In Publication 2, the predictions of the empirical ITB model are compared with the predictions from a theory-based fluid transport model (Weiland model).

In Publication 3, a comprehensive analysis and modelling of the impact of different current drive and heating methods on the q-profile evolution in the preheating phase are performed. Very recently, as an extreme example of the current profile modification by LHCD in the preheating phase, a so-called core current hole has been observed in JET. The core current hole has been investigated and modelled in Publication 4.

The effect of LHCD on the current profile and ITB formation in the main heating phase is investigated with transport simulations in Publication 5. Modelling shows that a significant increase in fusion performance in JET can be achieved with a proper current profile control by LHCD.

In Publication 6, the propagation and absorption of the LH waves in different plasma regimes, i.e. different density, temperature and different wave number spectrum of the LH wave, are studied. In addition, the general properties of the FRTC ray-tracing code are investigated in detail.

The author has actively participated in all the work reported in this thesis. He is the principal author in Publications 1–3 and 5. In Publications 1–5, he performed all the transport modelling calculations. He also carried out the empirical data analysis in Publication 1. In Publication 4, he carried out all the numerical transport simulations and contributed to the theoretical ideas behind the core current hole. In addition, he did the transport model and the LH module validation in Publication 5. In Publication 6, he performed all the LH ray-tracing and transport calculations as well as derived the accessibility regions for the LH waves. Other publications related to this thesis with a significant contribution from the author are in Refs. [95, 118, 124].

Contents

Chapter 1

Introduction

Energy consumption in the world is anticipated to double or even to triple within the next 50 years [1]. Firstly, the world population will increase significantly and secondly, the average power consumption per capita will also increase inevitably. However, the proven recoverable reserves of energy will suffice only for a limited time. At the present energy consumption rate, oil and natural gas as well as uranium used in light water nuclear reactors will exhaust within the next 100 years. Furthermore, if the share of fossil fuels remains at the present level, the risk of a major climate change due to the release of CO_2, possibly followed by catastrophic consequences on the environment, is high. Consequently, the development of energy sources with better compatibility with the environment and acceptable to society are needed. However, the number of conceivable non-fossil candidates, which in the long-term could substantially contribute to the energy production, is very limited — renewable energy sources such as solar and wind energy or totally another type of solution, nuclear fusion. Nuclear fusion is an environmentally friendly energy source with inexhaustible resources, well suitable for base load electric production. It is also inherently safe, the worst possible accident in a fusion reactor would not lead to evacuation of people living nearby. However, to exploit fusion, high technology is required, which makes fusion energy expensive compared with conventional energy sources. On the other hand, it is a huge challenge for science and big, almost impossible tasks are always wanted to be solved by scientists. In this thesis, one of the key difficulties in nuclear fusion, heat and particle transport, is explored.

1.1 Nuclear Fusion

In nuclear fusion, two nuclei of light elements are brought together within the range of their strong interactions. As a consequence, the nuclei react and melt together, forming new, heavier elements while also releasing the binding energy of the original nuclei. This reaction is the power source of the sun and other

stars, where confinement and heating occur through compression under enormous gravitational forces. Harnessing the energy of stars on the earth sets demanding requirements for the fuel temperature, density, and confinement in order to force positively charged particles to fuse at a rate that makes energy production possible.

The most accessible and promising reaction for fusion reactors is the one between deuterium D and tritium T. When these two nuclei fuse, the mass of the fusion products, i.e. the mass of a helium nucleus and a neutron is smaller than the mass of the fuel nuclei (deuterium + tritium) and therefore, according to Einstein's famous formula $E = mc^2$, energy is released as

$$ {}^{2}_{1}\mathrm{D} + {}^{3}_{1}\mathrm{T} \rightarrow {}^{4}_{2}\mathrm{He} + {}^{1}_{0}\mathrm{n} + 17.6\ \mathrm{MeV}. \tag{1.1} $$

As shown by Eq. (1.1), even a small amount of fusion fuel produces a huge amount of energy. For this reaction, the necessary requirement for the net energy production, i.e. break-even criterion (fusion gain Q exceeds 1 or $Q = P_{\mathrm{fus}}/P_{\mathrm{in}} > 1$ with P_{fus} and P_{in} being the fusion and input heating powers, respectively), sets the lower limit for the so-called fusion triple product as

$$ T_{\mathrm{i}} n_{\mathrm{i}} \tau_E > 1.0 \times 10^{21}\ \mathrm{keVm^{-3}s}, \tag{1.2} $$

where T_{i} is the ion temperature, n_{i} the ion density and τ_E is the energy confinement time. Worth noting is that in order to have the net energy production criterion valid, T_{i} must be larger than 10 keV. Typically the required ion temperature is of the order of $T_{\mathrm{i}} = 10$–30 keV, i.e. corresponding to about 100 million $^{\circ}C$. The energy confinement time is defined (in steady-state) as the ratio between the energy in the plasma $W = 3/2(n_{\mathrm{i}}T_{\mathrm{i}} + n_{\mathrm{e}}T_{\mathrm{e}})$ and the input heating power P_{in}, i.e. $\tau_{\mathrm{E}} = W/P_{\mathrm{in}}$. The energy confinement time is limited by the energy losses due to thermal conduction and convection processes and due to radiation. When a gas is heated to such a high temperature, atoms in a gas ionise, thus producing two populations, electrons and ionised atoms. This matter is defined to be plasma, sometimes also referred to as the fourth state of matter.

1.2 Plasma Confinement Systems for Nuclear Fusion

Since an extremely high temperature is needed for nuclear fusion, it is obvious that plasma confinement is not a trivial problem. For the present, there exist two main approaches to realise nuclear fusion — inertial and magnetic fusion. In inertial fusion, the Lawson criterion is approached by maximising the density n while having a relatively short energy confinement time τ_E. Inertial fusion consists of micro-explosions of small D–T fuel pellets by means of powerful lasers or particle beams. The fuel pellet reaches the required temperature and finally the burning pellet ignites. In magnetic fusion, hot plasma is confined with magnetic fields. On the contrary to the inertial fusion, density is now moderate, but the confinement time can be much longer, of the order of 1 s in the present fusion devices.

The most promising magnetic fusion device that could solve the confinement problem of the plasma is a tokamak [2, 3]. The basic idea of the tokamak was presented already in 1951 by the Russian physicists Tamm and Sakharov [4, 5]. In the first tokamak experiments, the net energy criterion was by a factor of 10^7 below the break-even condition. During the sixties the tokamak research spread over the whole world and led to rather pure plasmas with electron temperatures around 1 keV, and a confinement time of 7 ms was achieved in the T-3 tokamak [6]. By the seventies the tokamak concept was generally accepted and its significance appreciated. After the seventies the tokamaks have grown in size, and the net energy conditions have become even closer with the confinement time around 100 ms. The discovery of the high confinement mode (H-mode) on the German ASDEX (Axial Symmetric Divertor Experiment) tokamak in 1982 provided a new operating regime where the confinement time was increased significantly and the break-even condition became even closer [7]. So far the best fusion performance has been obtained in the largest currently existing tokamak JET (Joint European Torus) that is located near Oxford in the Great Britain. In the latest H-mode D-T experiments in JET in 1997, the following new records were achieved: transient fusion power of 16.1 MW with a fusion gain $Q = P_{\rm fus}/P_{\rm in} \approx 0.65$, quasi steady-state fusion power of 7 MW and fusion energy of 21 MJ [8]. In JET, the density is typically $\approx 5 \times 10^{19}$ m^{-3} at the ion temperature of 15–20 keV and the confinement time at best ≈ 0.5 s. As a consequence, for the moment JET is only about a factor of 2 separated from the net energy production condition given by the fusion triple product criterion in Eq. (1.2).

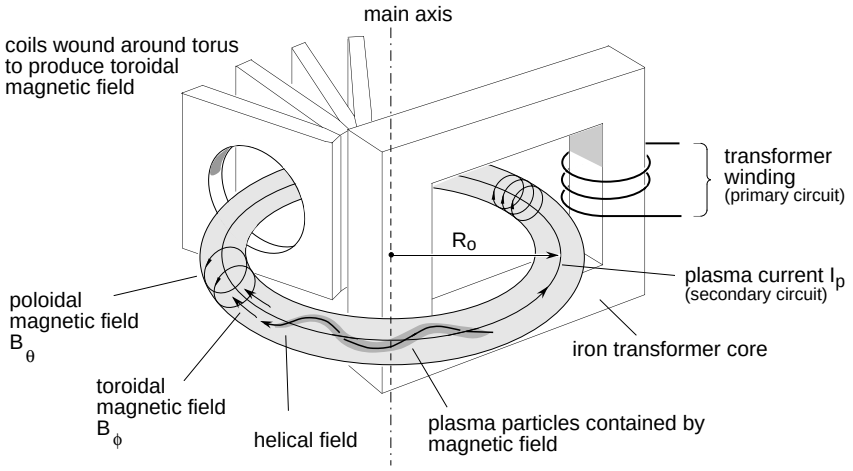

Figure 1.1: The tokamak, its magnetic fields and some of its subsystems. Adapted from Ref. [9].

The tokamak, a toroidal magnetic trap, is based on magnetic confinement where particles are trapped around the closed magnetic field lines as shown in Figure 1.1. The dominant toroidal magnetic field B_ϕ is generated by a toroidal field coil system. In order to prevent particles from drifting out of the plasma, a poloidal magnetic

field B_θ is also required. In a tokamak, this is done by creating a toroidal current I_p into the plasma. In a stellarator, which is the other main approach in magnetic fusion research, both the toroidal and poloidal magnetic fields are produced by external coils. The advantage of a stellarator is that there is no need to drive the toroidal current and thus, steady-state conditions are inherently present. Therefore, no such an event where the current and energy are suddenly lost, called a disruption, can occur. The drawback is an extremely complicated magnetic coil structure, which leads to even more challenging physics to understand than that in tokamaks.

Adding the poloidal magnetic field into the toroidal field in a tokamak, the resultant magnetic field is wound helically (i.e. is spiralled) around the plasma, as sketched in Figure 1.1. The magnetic winding number q expresses the number of toroidal orbits over the number of poloidal orbits, completed by a field line before it closes upon itself. The q-profile turns out to have a great impact on Magneto-Hydro-Dynamic (MHD) stability and transport and therefore, it is often called as the safety factor. It will be also one of the principal issues in this thesis.

1.3 Current Drive and Heating in a Tokamak

Traditionally, the toroidal plasma current is driven inductively so that the plasma operates as secondary circuit of a transformer as shown in Figure 1.1. When a current starts to run in the primary circuit, it induces an electric field in the plasma and further, the electric field creates the toroidal plasma current that is needed for the poloidal magnetic field. The plasma current produced with this method (called induction) is called Ohmic current. In order to maintain the electric field by means of induction, the current in the primary circuit system should be increased continuously. Since this is not realistic, a tokamak has to be driven in a pulsed mode. However, the pulsed tokamak operation mode is not desirable and therefore, large efforts are devoted to developing non-inductive current drive methods that would enable a tokamak fusion reactor to operate continuously. Even if the goal of the continuous tokamak operation is not fully achieved, non-inductive current drive is a necessary tool in modifying the current density profile. By modifying the current density profile, some MHD instabilities and turbulence can be suppressed.

The main idea of current drive is to introduce some kind of asymmetry in the velocity distribution of the electrons or ions in the toroidal direction which then leads to a toroidal current [10]. There are quite a few ways to generate this asymmetry. The methods to modify the current density profile can be divided into three different classes. Neutral Beam Current Drive (NBCD) and Radiofrequency (RF) current drive are based on external current drive and the third option, bootstrap current, is always inherently present in the tokamak operation.

In a tokamak plasma, the current drive and heating methods are closely related together. In all tokamaks, the initial heating comes from the dissipation of the Ohmic plasma current. However, the Ohmic heating decreases rapidly as the tem-

perature increases and temperatures of only 1–2 keV are achievable. Therefore, on top of the external current drive, external heating is also needed. In general, the difference between the external plasma heating and the external current drive is that in heating, both toroidal directions are treated in an equal manner whereas in current drive, one toroidal direction is favoured over the other. It is also to note that the current drive contributes to heating.

The heating by Neutral Beam Injection (NBI) is based on external injection of energetic neutral beam particles into the plasma, and on subsequent ionisation and slowing-down of these beam particles by Coulomb collisions with the background plasma. The ionised beam particles are then confined by the magnetic fields and accordingly, NBI fuels the plasma as well. Directing the beams with a component into one toroidal direction provides the neutral beam driven current. The radiofrequency heating and current drive involves high power electromagnetic waves launched into the plasma, tuned to some natural resonance frequency of the plasma, finally leading to absorption of the wave and transfer of its energy to the plasma particles. The main requirements for the radiofrequency heating are that it should be possible to launch a wave from an antenna or waveguide at the plasma edge and that the wave must be able to propagate to the central region of the plasma and be absorbed there [11]. Similarly to RF current drive, radiofrequency heating is useful in controlling the plasma profiles. The absorption of the RF waves can be localised and the radial position of the absorption is controllable, allowing it to be used to change the temperature or pressure profile. This is sometimes necessary in order to avoid MHD instabilities and suppress turbulence.

The schemes used in radiofrequency heating and current drive fall into three main frequency ranges. Heating in the lowest frequency range at a few tens of MHz is called Ion Cyclotron Resonance Heating (ICRH). This is the scheme that provides most of the RF heating power in present tokamaks, for example more than 10 MW in JET. The frequency of the waves in the Lower Hybrid Current Drive (LHCD) region is a few GHz. LHCD has turned out to have a key role in current drive and current profile modification for example in JET. When the frequency is further increased to about 100 GHz, Electron Cyclotron Resonance Heating (ECRH) and Electron Cyclotron Current Drive (ECCD) can be applied.

1.4 Plasma Transport

In order to achieve thermonuclear fusion conditions in a tokamak, it is necessary to confine the plasma energy for a sufficient time, as shown in Eq. (1.2). Confinement is limited by diffusion, convection and radiation losses. It can be improved by increasing the size of a tokamak or increasing the magnetic field. However, also the cost of a tokamak reactor scales with its volume and with the magnitude of the field. Therefore, understanding why the heat and particles move away from the centre of the tokamak, i.e. heat and particle transport, has a key role in the fusion research. Despite the huge efforts by the fusion scientists during the last decades, many

features of plasma transport still lack theoretical explanation. The diffusivities in all tokamaks exceed by large amount the predictions of the collisional transport theory. The increased transport is most likely due to plasma micro-turbulence, but the details have not yet been verified.

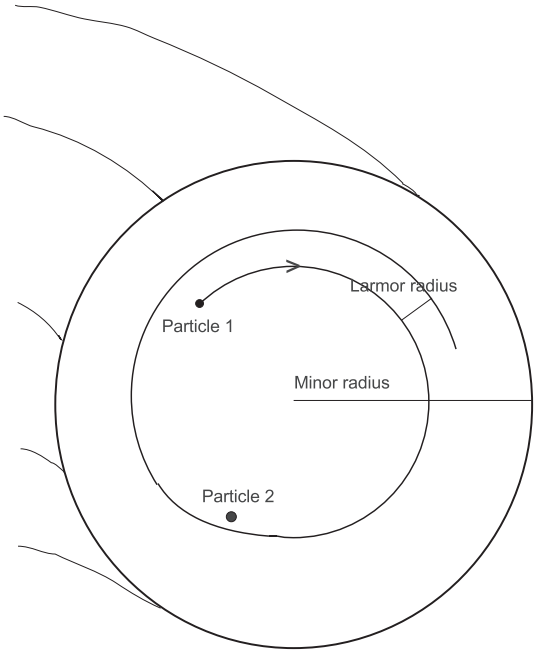

Figure 1.2: A particle experiencing a collision in a simplified cylindrical geometry.

Transport in a tokamak plasma is normally dominated by diffusion processes. The simplest approach to calculate the diffusion coefficients comes from the random-walk model. According to classical transport, which is the simplest model of transport, transport arises from the Coulomb collisions with other particles. In a cylinder with an axial magnetic field without collisions, the particles would move along the magnetic field lines. However, after experiencing a collision with another particle (time between consecutive collisions of a particle is defined as τ), the particles move a distance Δx from their initial field line across to the next field line. This is called transport. This typical random walk process is illustrated in the cross-section of a cylinder in a simplified way in Figure 1.2. Particle 1 moves along the magnetic field line around the cross-section of the cylinder until it comes in the vicinity of another particle 2. Then, it collides or scatters away by a distance of one Larmor radius ($\Delta x \approx r_{\mathrm{L}}$) and continues its trajectory there. The transport coefficient can be estimated by the random walk diffusion coefficient as

$$D_{\mathrm{class}} = (\Delta x)^2/\tau = \nu r_{\mathrm{L}}^2, \tag{1.3}$$

where $\nu = \tau^{-1}$ is the collision frequency of the particles and r_{L} the Larmor or the gyroradius of the particle. Transport by this mechanism in a cylindrical geometry, where the magnetic field lines are straight, is called classical transport

(D_{class}). In a real tokamak plasma, there is a large number of ions and electrons colliding with each other and each collision leads to different scatter and losses. Therefore, the real calculation procedure is very complex. Furthermore, for typical plasma parameters, as for example in JET, the classical diffusion coefficient is several orders of magnitude smaller than the experimentally observed diffusion coefficients. Therefore, classical transport is far from satisfactory to explain the tokamak transport.

The real tokamak geometry is not cylindrical but toroidal, and the toroidal geometry allows the coupling of parallel and perpendicular dynamics. This coupling increases the transport significantly. In addition, the viscosity in a toroidal geometry leads to an additional increase in transport. Transport in a torus, where the magnetic field lines are curved, is called neo-classical transport [12]. In a toroidal tokamak geometry, the particle trajectories remind of the shape of the banana and thus, the particle orbits are called as banana orbits. According to the collisionality, neo-classical transport can be divided into three regimes. In the Pfirsch-Schlüter regime, the collisionality is so high that a particle cannot complete a banana orbit without a collision whereas in the banana regime, collisionality is so low that a particle can well complete the banana orbit. Between the two limiting cases is the Plateau regime.

In the random-walk process, the reason for the enhanced transport comes from the increased step size (Δx) due to trapped particles. The trapped particles are those particles that are trapped on the low field side with their orbits having the shape of the banana. The step size of the trapped particles in the banana regime is larger than the gyroradius. The increase in the neo-classical transport compared with the classical transport due to the toroidal geometry effects can be written as

$$D_{\mathrm{neocl}} = G \times D_{\mathrm{class}} = G \times \nu r_{\mathrm{L}}^2, \tag{1.4}$$

where G stands for the geometry factor. G is either $2q^2$ (in the Pfirsch-Schlüter regime), $2q^2\epsilon^{-3/2}$ (in the Banana regime) or $v_{\mathrm{th}}q^2/(qR\nu)$ (in the Plateau regime), depending on the collisionality of the plasma. Here, ϵ is the inverse aspect ratio $\epsilon = r/R$ with R and r referring to major and minor radii and v_{th} and ν are the thermal velocity and collisionality, respectively. D_{neocl} is typically a factor of 10–100 larger than D_{class}. In a simplified geometry, analytical estimates for the neo-classical transport coefficients exist under certain approximations [12, 13, 14]. Neo-classical theory yields for a tokamak typically the following values: $D_{\mathrm{neocl}} \approx \chi_{\mathrm{e,neocl}} \approx \chi_{\mathrm{i,neocl}}\sqrt{m_{\mathrm{e}}/m_{\mathrm{i}}} \approx 0.01$ m^2/s with m_{e} and m_{i} being the electron and ion mass, respectively. $\chi_{\mathrm{e,neocl}}$ and $\chi_{\mathrm{i,neocl}}$ are the neo-classical electron and ion heat transport coefficients and D_{neocl} the neo-classical particle transport coefficient.

Neo-classical transport is regarded as the minimum level of transport in tokamak plasmas, i.e. values of real diffusivities should be equal to or larger than the neo-classical predictions. Experiments on various tokamaks show that energy losses via the electron channel exceed the neo-classical predictions by one or two orders of magnitude, while the losses via the ions are reported to be roughly one order of magnitude larger than the neo-classical predictions. The transport coefficients in tokamaks are typically of the order 1 m^2/s, rather than 0.01–0.1 m^2/s as predicted

by the neo-classical theory. Micro-turbulence in electric and magnetic fields, not taken into account by the neo-classical theory, is regarded to be responsible for the increased transport. This increased transport is called anomalous transport.

Much effort has been put into the study of the anomalous transport during the last ten years. The ultimate goal of this effort is to understand micro-turbulence and turbulent transport, how to control it and how to achieve important reductions in the anomalous transport. Fortunately, some mechanisms that suppress turbulence and thus reduce the anomalous transport have been found. As already mentioned earlier, the discovery of the high confinement mode (H-mode) in 1982 provided a new operating regime where the turbulence in the edge region of the plasma is suppressed [7]. The discovery of the Edge Transport Barrier (ETB), i.e. H-mode, led to significantly longer confinement times and reduced transport coefficients. In the mid 1990s, several tokamaks, like JT-60U [15], TFTR [16], DIII-D [17], and JET [18, 19] reported confinement levels by a further factor of about two above the standard H-mode level. Turbulence had been suppressed in the core region of the plasma and anomalous transport further reduced besides the ETB — an Internal Transport Barrier (ITB) had been found. After the suppression of turbulence by the internal transport barrier, the transport level, in particular in the ion channel, may be reduced down to the neo-classical level in the plasma core [20, 21, 22, 23, 24]. The characteristics of the ITBs are the reduced heat and/or particle diffusivity and the increased gradients in T_i, T_e and n_e in the core region. This enhanced operation mode with the improved core confinement due to ITBs, together with the modified current density profile, is called as the 'Advanced Tokamak Scenario'.

In the transport theory, the particle transport, the ion and electron heat transport and transport of the toroidal current are coupled. The basic idea in the neo-classical transport theory is to find linear relations between fluxes, such as the heat or particle flux, and thermodynamical forces, like the temperature or density gradient. This coupling can be described in a form of the matrix equation as follows:

$$\begin{pmatrix} \Gamma/n \\ q_\mathrm{e}/(nT_\mathrm{e}) \\ q_\mathrm{i}/(nT_\mathrm{i}) \\ j \end{pmatrix} = \begin{pmatrix} D & L_{21} & L_{31} & L_{41} \\ L_{12} & \chi_\mathrm{e} & L_{32} & L_{42} \\ L_{13} & L_{23} & \chi_\mathrm{i} & L_{43} \\ L_{14} & L_{24} & L_{34} & \sigma \end{pmatrix} \begin{pmatrix} n^{-1}\nabla n \\ T_\mathrm{e}^{-1}\nabla T_\mathrm{e} \\ T_\mathrm{i}^{-1}\nabla T_\mathrm{i} \\ E \end{pmatrix}. \tag{1.5}$$

Here Γ, q_e and q_i are the particle flux and the electron and ion heat fluxes, respectively, and j and E are the toroidal current density and electric field, respectively. The diagonal terms describe the diffusion with D being the particle diffusion coefficient, χ_e and χ_i the electron and ion heat diffusion coefficients and σ the electrical conductivity. The off-diagonal or pinch terms L_{ij} couple for example the particle flux to the temperature gradients and vice versa. In typical tokamak plasmas, these off-diagonal terms are much smaller than the diagonal terms. Some of them are, however, of great importance, like the off-diagonal term L_{14} which indicates that the density gradient drives current. This current is called the bootstrap current which was already mentioned in Section 1.3 (also the temperature gradients drive bootstrap current, thus L_{24} and L_{34} are non-zero). Since up to a suitable normalisation the transport matrix has the onsager symmetry, i.e. $L_{14} = L_{41}$, the electric

field must drive particle flux. This particle flux is called the Ware pinch. The determination of the diffusivities has long been one of the primary goals in transport studies. In determining the transport coefficients, there are three possible ways of making progress — theoretical, numerical simulations and experimental. The methods used in this thesis are concentrated on numerical simulations, but also experimental and theoretical aspects are considered.

1.5 Outline of This Thesis

This thesis is an introduction to and review of Publications 1–6. The two central questions that form the basis of this thesis are the following ones: firstly, how can ITBs be modelled and predicted and secondly, how do different current drive and heating systems affect the q-profile evolution and further the ITB dynamics in the 'Advanced Tokamak Scenarios'. Consequently, the key issues in these publications are modelling of transport and internal transport barriers as well as modelling of current drive and heating.

A schematic view of various interactions constituting a tokamak energy balance is illustrated in Figure 1.3. The grey boxes in the middle describe the energy and particle content of the electrons and ions, and the solid and dashed arrows indicate the energy and particle flows, respectively. The predominant heat and particle loss mechanism in a tokamak is the radial transport or just shortly transport. Transport itself is further dominated by the diffusion processes (diagonal terms in Eq. (1.5)). The work carried out in this thesis is to resolve some of the numerous questions involved in the incomplete picture of the transport, in particular the internal transport barriers, in tokamaks. The ITB formation mechanisms as a function of local plasma parameters, i.e. the threshold where confinement improves and transport reduces in the core region, are sought in plasmas of the JET tokamak (Publication 1). In addition, quantities that govern the further time evolution of the ITBs in JET are investigated.

After having found the empirical ITB formation threshold condition in JET, the threshold condition is implemented into the semi-empirical Bohm/GyroBohm transport model [25, 26]. The empirical ITB threshold condition is then tested against a large database of JET ITB discharges with JETTO [27] transport code. The predictions of the empirical ITB model are also compared with the predictions of the theory-based fluid transport model (Weiland model) [28, 29, 30, 31] in Publication 2. This transport model comparison sheds light on the possibility of having several different ITB formation mechanisms producing fairly similar results.

The source terms for the electron and ion energy are described by the boxes on the left-hand side of the grey boxes in Figure 1.3. The ohmic and externally driven current are also provided by these heat and particle sources. As it was deduced in Publication 1, the magnetic shear s, i.e. the derivative of the safety factor $s \approx (r/q)(dq/dr)$, is one of the key elements in the formation of the ITB in

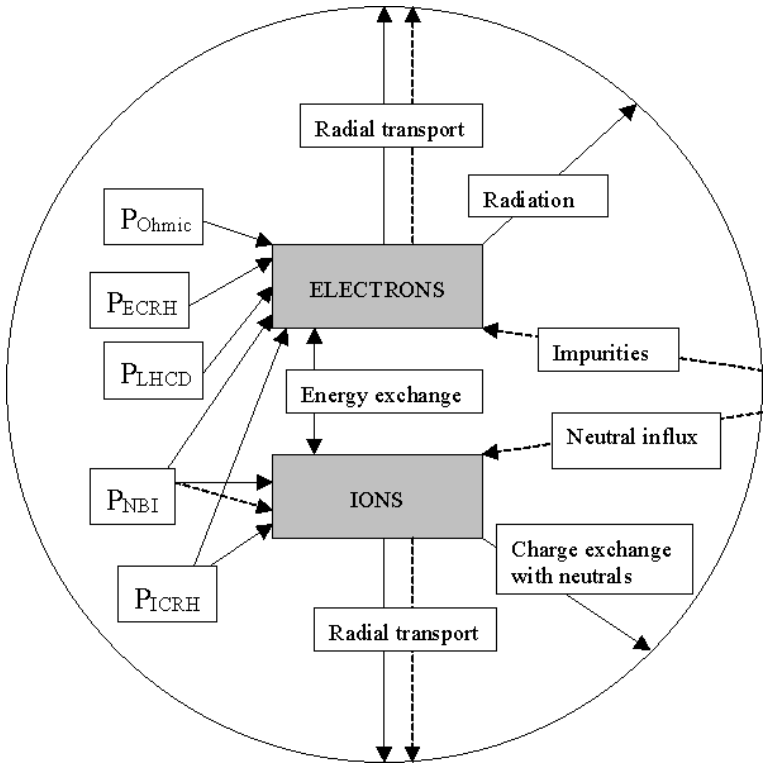

Figure 1.3: A scheme of the various interactions constituting an energy and particle balance in a tokamak.

JET. As a consequence, modifying the current density profile, which determines the q-profile, has a large impact on triggering the ITB. This was the motivation to a comprehensive analysis and modelling of the impact of different current drive and heating methods on the q-profile evolution performed in Publication 3. The modelling is based on JETTO transport code to which different heating and current drive modules, such as FRTC [32] (LHCD ray-tracing code), ECWGB [33] (ECRH beam-tracing code) and PENCIL [34] (NBI code), are coupled. FRTC and ECWGB modules were installed and tested in JETTO during the course of this thesis.

As confirmed by the results in Publication 3, LHCD is very suitable for current drive and current profile modification in JET. Therefore, a more detailed study on the effect of LHCD on the current profile and ITB formation is performed in Publication 5. Modelling shows that a significant increase in fusion performance in JET can be achieved with a proper current profile control by LHCD. Very recently, as an extreme example of the current profile modification by LHCD, a so-called core current hole has been observed in JET (Publication 4). It arises from a fast current ramp-up together with a simultaneous application of LHCD at low electron density. The transport analysis of the core current hole with the coupled JETTO/FRTC code

reported in Publication 4 is in a good agreement with experiments — it shows the wide region ($r/a \leq 0.2$) of zero current density in the plasma core, similarly to experimental measurements. The propagation and absorption of the LH waves in different plasma regimes, i.e. different density, temperature and different wave number spectrum of the LH wave, as well as the general properties of the FRTC code are studied in detail in Publication 6.

This thesis is organised in the following way. The general issues of the 'Advanced Tokamak Scenarios' are illustrated in Chapter 2. In addition, the main transport mechanisms and transport barriers are presented. In particular, the mechanisms that affect the ITB formation, further time evolution and a collapse are discussed in Section 2.3. Moreover, the results from the empirical study of the local plasma parameters governing the ITB formation in JET are shown. In Section 2.4, the numerical codes and transport models used during the course of this thesis are presented. Chapter 3 is devoted to reporting the modelling results from various kinds of transport simulations. In Section 3.1, the main emphasis is in the predictive modelling of the formation and dynamics of the ITBs. The results from the ITB modelling in JET are compared with results from other transport models in other tokamaks. In Section 3.2, the transport simulations of the current density profile, both in the preheating and main heating phases, are presented. Finally, the conclusions with a summary are discussed in Chapter 4.

Chapter 2

Advanced Tokamak Scenarios with Internal Transport Barriers

In the so-called 'Conventional Tokamak Scenarios', the plasma current is driven inductively. It is the most thoroughly investigated tokamak scenario and consequently, it has been chosen as the primary operation mode for the next step tokamak, International Thermonuclear Experimental Reactor (ITER) [35]. There are several reasons why the 'Conventional Tokamak Scenario', often also referred as the 'ELMy H-mode Scenario' has been chosen as the main operation mode. The ELMy H-mode here means the tokamak operation in the H-mode with Edge Localised Modes (ELMs) governing the physics of the edge of the plasma. Firstly, the H-mode is robust, having been seen under a wide variety of conditions in a large number of tokamaks. In addition, the ELMy H-mode scenario has been run in steady-state for as long as 20 s on JET [36]. Here, steady-state means that the temperature, density and current density profiles do not change significantly in time. The ELMy H-mode scenario also exhibits good confinement even in high density cases where the electron and ion temperatures are equilibrated — this is consistent with alpha particle heating and thus needed for ITER. Furthermore, the ELMy H-mode scenario has flat density profiles in the plasma core which are important in order to prevent impurity and helium accumulation in the core, as demonstrated in DIII-D [37]. Finally, the ELMy H-mode scenario requires no special current profile control for long pulse operation, unlike the 'Advanced Tokamak Scenarios'.

On the other hand, the 'Conventional Tokamak Scenario' has its drawbacks as well. Since a large fraction of the plasma current is driven inductively, very long steady-state operation (of the orders of hours or days in a fusion reactor) would not be possible. Moreover, since the device has to operate in a pulsed mode, in a power

plant an energy storage system is required to avoid the loss of the power production capacity during the burn-off phase. In addition, pulsed reactors have large unit size with low fusion power density whereas the utilities would prefer power plants of modest ($\leq$ 500 MW) unit size to match the power production with the demand and to have lower capital investment. In addition, the thermocyclic loads between the burn and burn-off phases become unbearable. Therefore, the 'Conventional Tokamak Scenario' is probably not a feasible operation mode in a commercial fusion reactor. In view of these very serious drawbacks, the fusion community has started to develop more attractive tokamak reactor scenarios, called the 'Advanced Tokamak Scenarios'.

The fundamental ideas in the 'Advanced Tokamak Scenarios' towards an attractive tokamak reactor are to reduce the size of the tokamak (or to increase the margins at a given size), to increase the fusion power density, to improve confinement with internal transport barriers and to drive a large fraction of the total current as bootstrap current to render the tokamak compatible with continuous operation. The main means to achieve these goals are to optimise the shape of the current density (i.e. q-profile) and pressure profiles by external current drive and heating as well as by the optimal alignment of the large fraction of the bootstrap current. A flat or reversed q-profile facilitates the formation of the internal transport barriers which are crucial for significant improvements in confinement and bootstrap current fraction in the 'Advanced Tokamak Scenarios' [16, 17, 19, 38]. Record fusion performance in DIII-D and JT-60U has been achieved utilising the 'Advanced Tokamak Scenarios' [39, 40]. As a consequence, the 'Advanced Tokamak Scenario' research concentrates on the studies of the ITB formation and dynamics as well as the current profile control by external current drive. These two actual topics are also the main issues in this thesis. Other important issues in the studies of the 'Advanced Tokamak Scenario' are the optimisation of the plasma shape as well as the heat and particle exhaust and avoidance and mitigation of detrimental MHD instabilities, like the large-amplitude neo-classical tearing modes and giant ELMs.

2.1 Transport in a Tokamak

Understanding of plasma transport is an issue of paramount importance, both in the 'Conventional' and 'Advanced Tokamak Scenarios', for a design of a future tokamak reactor. Anomalous transport, together with some major MHD instabilities, controls plasma confinement, transport and overall fusion performance. It is universally recognised that transport properties vary a lot across the plasma so that it is constructive to subdivide the plasma volume in radius into five regions with different transport characteristics [41]. The schematic view of such a division is shown in Figure 2.1. All the three most common operation modes, i.e. the L-mode, the 'Conventional Tokamak or the ELMy H-mode Scenario' and the 'Advanced Tokamak Scenario, are illustrated. The difference between the L-mode (dotted line) and the H-mode (dashed line) is the edge transport barrier, which improves the energy confinement by a factor 2–3. The L-mode operation used to

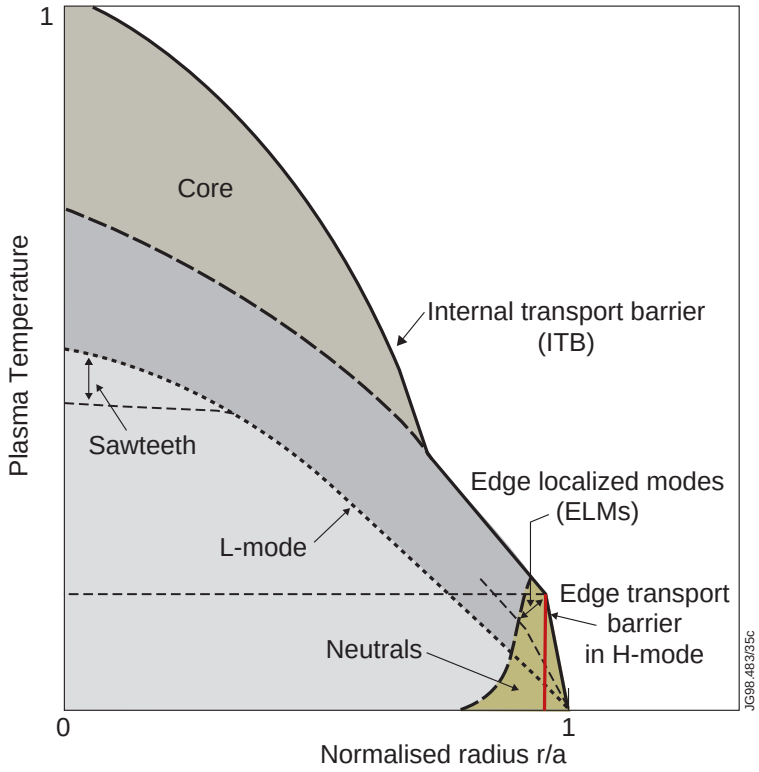

Figure 2.1: Schematic view showing the five different regions with different transport characteristics in a tokamak. Adapted from Ref. [41].

be the most common operation mode, but for the present it is not regarded as an attractive approach towards an economic fusion reactor. An ITB separates the 'ELMy H-mode Scenario' from the 'Advanced Tokamak Scenario' (solid line). The improvement in confinement due to an ITB is typically a factor of 2–3.

Starting from the edge, region 1 is the Scrape-Off-Layer (SOL), which represents the plasma outside the separatrix ($r/a > 1$). Transport properties in this region are dominated by the fast parallel transport and by the atomic physics processes. Region 2 is the Edge Transport Barrier (ETB) region that is a narrow region just inside separatrix. When an ETB exists, i.e. when the H-mode exists, significant reductions in the micro-turbulence level are observed. Transport in region 2 is dominated by the physics of the ETB and by ELMs. The intermediate region 3 ($0.8 \leq r/a \leq 0.95$) links the core plasma to the edge. ELMs, collisional turbulence and cold neutrals dominate transport in region 3. Deeper in the core (between $0.4 \leq r/a \leq 0.8$) is region 4 which is usually free from any strong MHD instabilities. Its transport is dominated by drift type of micro-turbulence [42, 43, 44]. This is also the region where an internal transport barrier normally forms and exists. Finally, transport in the central part of the plasma in region 5 (inside $r/a \leq 0.4$)

is either dominated by MHD events, called sawteeth, in the 'Conventional Tokamak Scenario' or with reduced micro-turbulence and neo-classical transport in the 'Advanced Tokamak Scenario' with ITBs. Sawtooth is usually absent in the 'Advanced Tokamak Scenario' because the standard condition to have sawteeth ($q < 1$) is not fulfilled in those plasmas. In this thesis, the main emphasis in transport modelling and data analysis is focused on the central and core regions (regions 4 and 5, $0.0 \leq r/a \leq 0.8$) although the numerical simulations are extended up to $r/a = 1.0$. Transport in regions 4 and 5 is dominated by the micro-turbulence and ITB physics in the 'Advanced Tokamak Scenarios'. However, both experimental evidence and theoretical considerations suggest that the underlying transport properties are strongly linked between all the five regions. Still, it is quite justified to study anomalous transport in each or in some of the regions independently.

As already mentioned, anomalous transport dominates in regions 4 and 5. There are two main routes in seeking after the explanation of the anomalous energy and particle losses observed in tokamaks. In the first picture, anomalous transport results from fluctuations in the electric field due to fluctuations in density and temperature. The fluctuating electric field leads to small scale $E \times B$ drifts [2, 29, 45, 46]. This is referred to as 'electrostatic turbulence'. The other picture explains the anomalous transport by fluctuations in the magnetic field, referred to as 'magnetic turbulence' that can break the toroidal symmetry and destroy the nested flux surfaces [47]. Since the heat conductivity parallel to the magnetic field is many orders of magnitude higher than perpendicular, the particles flowing along the magnetic field lines reach the plasma edge very fast in the case of broken flux surfaces. It is remarked that even if any physical fluctuation has both the electrostatic and magnetic components, the classification is nonetheless a useful one. Since a tokamak plasma is a combination of several fluids, the plasma turbulence is a result from fluctuations of these multiple turbulent fluids coupled through electromagnetic, friction and energy exchange effects. It is not surprising, therefore, that there is not yet a theory or even a comprehensive approach to this problem.

2.1.1 Heat Transport

The heat transport in the core region of the tokamak is mainly anomalous although the neo-classical transport may be important for the ion heat transport in some special cases. The heat transport caused by the turbulence is driven by the free energy sources of many plasma micro-instabilities, essentially the gradients of the temperature and density [48]. In the plasma core, the micro-instabilities are classified into three categories according to the source of the free energy; instabilities driven by the ion temperature gradient, instabilities driven by the electron temperature gradient and fluid-like instabilities driven by the pressure gradient. The most investigated micro-instability is the Ion Temperature Gradient (ITG) drift mode. It has the longest wavelength amongst the different branches of the micro-instabilities and it is believed to be the main contributor to the ion heat transport in tokamaks, but it is also known to affect the electron heat transport. The importance of the contribution from the ITG turbulence to the ion heat transport

is also recognised in the empirical study in Publication 1. The second category consists of the electron temperature gradient driven instabilities; Trapped Electron Modes (TEM) and Electron Temperature Gradient modes (ETG). The ETG has the shortest wavelength and the wavelength of the TEM is between the ITG and the ETG. The TEM has been found to be the dominant contributor to the heat transport in TFTR [49]. All the main branches of the instabilities, i.e. the ITG, the TEM and the ETG, contribute to the electron heat transport whereas the ETG does not contribute to the ion heat transport nor particle transport [50]. Fluid like instabilities, such as the current diffusive ballooning [51], drift resistive ballooning [52] and neo-classical tearing modes [53] belong to the third category of pressure driven instabilities.

In general, the drift turbulence becomes unstable only if the relevant relative temperature gradient exceeds the corresponding critical value of that instability. For example, the critical temperature gradient length for the ITG in the case of a flat density profile can be written in a simplified form according to Ref. [43] as

$$L_{\mathrm{T_i}}^{\mathrm{crit}} = \left| \frac{T_\mathrm{i}}{\nabla T_\mathrm{i}} \right|_{\mathrm{crit}} \approx R \frac{9}{20} \frac{T_\mathrm{e}}{T_\mathrm{i}}. \tag{2.1}$$

The existence of the critical temperature gradient of the micro-turbulence implies that there is a strong link between the edge and core. It is called as profile stiffness or profile resilience. This phenomenon has been observed on many tokamaks in which the ion and sometimes the electron temperature change in a self-similar way in the core, i.e. the core temperature is proportional to the edge temperature [54, 55]. The dependence of the core ion temperature on the edge temperature for a series of JET discharges with different edge ion temperatures is illustrated in Figure 2.2.

Theoretically stiffness can be explained by the fact that the drift turbulence becomes unstable only if the relevant relative temperature gradient exceeds some critical level $|\nabla T/T| \geq |\nabla T/T|_{\mathrm{crit}}$. In terms of transport or diffusion coefficient, the existence of the critical temperature gradient or stiffness for the ITG turbulence can be illustrated in the following way:

$$\chi_\mathrm{i}^{\mathrm{ITG}} \approx CR/a\rho_\mathrm{i}^2 v_{\mathrm{Ti}} \times \left(\left| \frac{\nabla T_\mathrm{i}}{T_\mathrm{i}} \right| - \left| \frac{\nabla T_\mathrm{i}}{T_\mathrm{i}} \right|_{\mathrm{crit}} \right), \tag{2.2}$$

where the multiplier $CR/a\rho_\mathrm{i}^2 v_{\mathrm{Ti}}$ indicates the widely accepted paradigm that a drift wave turbulence generates GyroBohm type of transport with ρ_i^2 and v_{Ti} being the ion gyro radius and the ion thermal velocity and C is a numerical constant. If $|\nabla T_\mathrm{i}/T_\mathrm{i}| \leq |\nabla T_\mathrm{i}/T_\mathrm{i}|_{\mathrm{crit}}$, no unstable ITG modes exist and $\chi_\mathrm{i}^{\mathrm{ITG}}$ is zero. The critical temperature gradient lengths are distinct for the ITG, TEM and ETG and therefore, typically only either the ion or the electron transport exhibits profile stiffness. Worth mentioning here is that stiffness observed regularly in the ELMy H-mode scenario is broken by the internal transport barriers in the core in the 'Advanced Tokamak Scenarios'. The ITBs will be discussed in detail in Secs. 2.2 and 2.3.

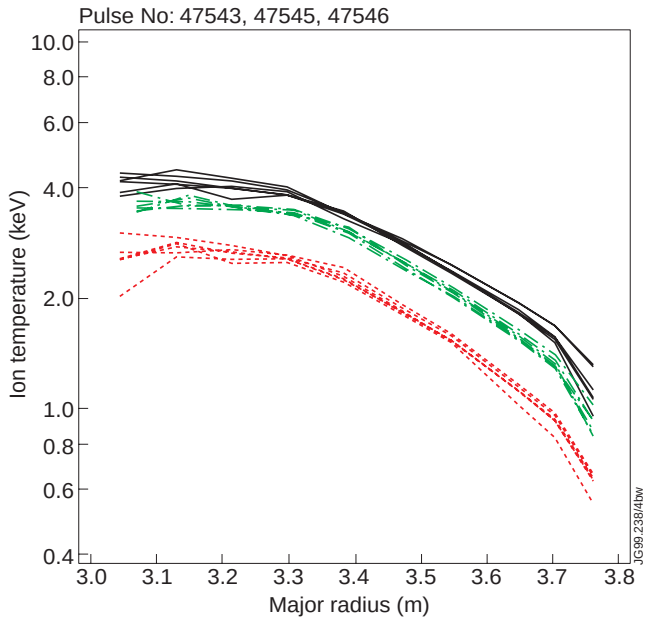

Figure 2.2: Ion temperature profiles for a series of JET shots with different edge ion temperatures indicating the profile stiffness. Adapted from Ref. [55].

Finally, it is instructive to list some experimental characteristics of the heat transport and confinement. The theory of the electrostatic turbulence predicts GyroBohm-like scaling and local transport, but it has been observed that the wavelength of the turbulence increases with increasing size of the tokamak — this is, however, an indication of Bohm-like scaling and non-local transport. Moreover, experiments with inward propagating heat and cold pulses have shown features that cannot be explained within the framework of local transport theory [56]. Consequently, transport has both local and non-local features. Another important observation is that the energy confinement time τ_{E} decreases with auxiliary heating power as $\tau_{\mathrm{E}} \propto P_{\mathrm{in}}^{-0.5}$. Fortunately, it increases with the isotope mass [57].

2.1.2 Particle and Momentum Transport

The particle transport models must be tailored in a different way for each particle species considered. Transport of electrons and deuterium and tritium ions is predominantly anomalous whereas the neo-classical effects play an important role in impurity transport. In this thesis, the electron and the ion particle transport are considered and taken into account in all the simulations and analyses whereas helium and impurity transport are not dealt with. However, still worth mentioning is the fact that in particular in the 'Advanced Tokamak Scenarios', the impurity and helium accumulation (in DT-plasmas) in the plasma core may ultimately be the

most strict condition that determines what kind of temperature, density and current density profiles are feasible in plasmas with ITBs. The impurity accumulation in the plasma centre is due to peaked density profiles arisen from steep pressure gradients of the ITBs.

The particle (electron and ion) transport is much less studied and also much less understood than the heat transport. Theoretically the particle transport is complicated due to ambipolarity, which means that particle diffusion is controlled by the least mobile component, usually electrons. Experimentally the particle transport sets up challenging requirements for the diagnostics in order to have time dependent measurements. Furthermore, cold recycled neutrals from the edge are distributed poloidally asymmetrically and therefore, their behaviour is difficult to measure or calculate.

Even if the particle transport is not well-known, some general remarks can be made. Firstly, plasma confinement degrades when plasma approaches the density limit, called the Greenwald limit [58, 59]. Secondly, the off-diagonal terms in the transport matrix (Eq. (1.5)) may play a larger role than in the overall heat transport [60]. In addition to the neo-classical Ware pinch mentioned in Section 1.4, anomalous pinch, in particular in the outer region of the plasma may be of importance. Furthermore, the role of convection is often significant in the particle transport. Thirdly, experiments indicate a strong correlation between the local thermal and particle transport properties in the core, normally the particle diffusivity aligned more closely with the ion thermal diffusivity ($D/\chi_\mathrm{i} \approx 1$), but sometimes also with the electron thermal diffusivity ($D/\chi_\mathrm{e} \approx 1$) [61].

The study of the toroidal plasma rotation or the toroidal velocity is of interest for several reasons. Firstly, plasma rotation contributes to the suppression of turbulence by the $\omega_{\mathrm{E}\times\mathrm{B}}$ flow velocity shear. This is the topic in Section 2.3.1. Secondly, the toroidal rotation can suppress the growth of the error field instability and improve the stability of low n-kink modes. Thirdly, the toroidal rotation transport studies can provide further knowledge of transport in a tokamak. The rotation in the poloidal direction is also important. According to the neo-classical theory, the magnitude of the poloidal rotation is proportional to the ion temperature gradient and it acts, like the toroidal rotation, as a suppression mechanism of micro-instabilities.

The momentum and energy confinement times have been found to have similar magnitudes on many tokamaks [62]. Experimental values of the toroidal momentum diffusivity χ_ϕ are significantly higher than the neo-classical gyro-viscosity — transport of the toroidal momentum is mainly anomalous. On the contrary, neoclassical transport determines mainly the poloidal rotation [63]. The ITG based gyroBohm theory leads to the equality $\chi_\phi = \chi_\mathrm{i}$ [64]. Experimental results on JET and TFTR also confirm that the radial profiles of the ion heat and toroidal momentum diffusivities are close to each other [65, 66].

2.1.3 Current Diffusion

The diffusion of the plasma current is one of the few transport processes in a tokamak that is believed to be almost purely neo-classical. In a cylindrical plasma, the classical electrical resistivity was derived already 50 years ago by Spitzer [67]

$$\eta_{\mathrm{s}} = 1.65 \times 10^{-9} \ln\Lambda / T_{\mathrm{e}}^{3/2}, \tag{2.3}$$

where the Coulomb logarithm $\ln\Lambda \approx 17$ and is a weak function of density. The classical resistivity is valid only for pure hydrogen plasma without any magnetic field. However, usually tokamak plasmas consist of hydrogen and deuterium with small fractions of impurities, thus having $Z_{\mathrm{eff}} > 1$, where Z_{eff} is defined as

$$Z_{\mathrm{eff}} = \frac{1}{n_{\mathrm{e}}} \sum_{i=1}^{N} n_i Z_i^2. \tag{2.4}$$

Here, n_i and Z_i are the density and charge of the main and the impurity ion species. In addition to the increase of η_{s} by $Z_{\mathrm{eff}} > 1$, trapped particles present in a toroidal device do not carry a current and the Spitzer resistivity is further modified to the neo-classical resistivity η according to [12, 13]

$$\eta \approx N(Z_{\mathrm{eff}}) Z_{\mathrm{eff}} \frac{\eta_{\mathrm{s}}}{[1-(r/R_0)^2]^2}, \tag{2.5}$$

where $N(Z_{\mathrm{eff}})$ decreases roughly from 1 to 0.5 when Z_{eff} increases from 1 to ∞ and $1/[1-(r/R_0)^2]^2$ is an approximation for the trapped particle correction. The simulated current diffusion by using either the Spitzer or the neo-classical resistivity are compared with the experimentally measured current diffusion in Publication 3. The comparison confirmed that the current diffusion on JET can be described very well by the neo-classical resistivity.

There are at least two occasions where the current diffusion is not neo-classical. Firstly, in the case of the sawtooth MHD instability, i.e. when $q < 1$ in the plasma centre, the current is redistributed in the plasma core with a MHD time scale that is much faster than the neo-classical current diffusion time. Secondly, very recently with a deeply reversed q-profile in the plasma core, it has been observed that there is sawtoothlike behaviour appearing in the electron temperature profiles although the condition to have the sawtooth instability active, i.e. $q < 1$, is not fulfilled [68]. This behaviour may lead to a partial redistribution of the current with a very fast time scale. The topic of the deeply reversed q-profile and its impacts are considered in Publication 4.

2.2 Transport Barriers

Progress in reducing the anomalous transport in tokamaks has been dramatic. The improvements in confinement, fusion performance and plasma stability due to

transport barriers have been drastic. Moreover, the richness of the physics revealed by these developments open the possibility of achieving deeper understanding of non-linear turbulent plasma phenomena.

2.2.1 Edge Transport Barrier

The high confinement mode (H-mode) associated with the formation of an edge transport barrier was first discovered in ASDEX in 1982 [7]. The ETB in the H-mode can be seen as steep temperature and density gradients just inside the separatrix at $r/a \approx 0.97$ in Figure 2.1. The H-mode exhibits global energy confinement about a factor of two better than the L-mode. Part of this is due to the formation of the ETB itself, however, another very important part is due to the reduction of the local transport throughout the whole plasma. Reductions in the electron and ion thermal diffusivity as well as in the angular momentum diffusivity have been observed. Although the ETB formation and the physics of the ETB and H-mode are beyond the scope of this thesis, the physics of the ETB and ITB may have similarities. Thus, it is worth mentioning that the leading hypothesis to date for the reappearence of the H-mode is the reduction of turbulent transport by the shear in $E \times B$ flow [69].

2.2.2 Internal Transport Barrier

In the middle of 1990s, many tokamak research groups reported that there is, in addition to the H-mode, also improved confinement in the core of the plasma [15, 16, 17, 18]. This improved core confinement is caused by an internal transport barrier and it is seen as larger temperature, density and pressure gradients in the core region in Figure 2.1 when compared with the standard H-mode.

ITBs and ETBs are now widely achieved in a number of devices with various control schemes, such as NBI heating, ICRF and ECRF heating, LHCD, momentum and mass injection etc. This suggests that there may be several mechanisms that can trigger barriers and affect the dynamics of the barriers. This is discussed in more detail in Section 2.3. Furthermore, there are some similarities in the radial structure of the ETB and ITB, and these similarities point to common physics involved in the formation and sustainment of the barriers. One of them is the qualitatively similar structure of the radial electric field E_r at both the ETB and the ITB [70].

The radial location of the ITB is usually between $0.2 \leq r/a \leq 0.8$. The location can vary with time — roughly speaking the location of the ITB moves inwards when heating is decreased and outwards when heating is increased. Naturally, other quantities, like the q-profile and the radial electric field, affect the actual evolution of the location of the ITB, this is discussed in more detail in Section 2.3.

ITBs have been observed simultaneously in all the four transport channels, i.e. in the ion and electron heat transport as well as in the electron particle and angular

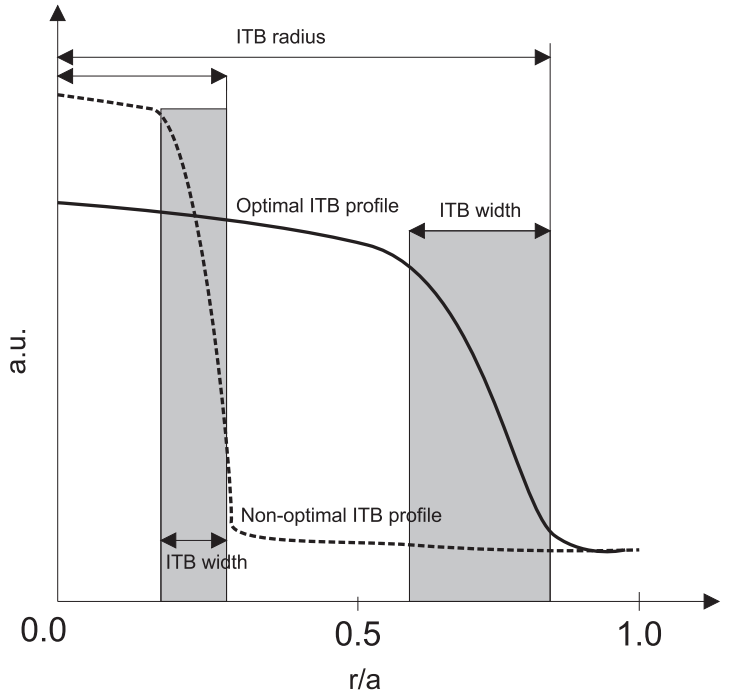

Figure 2.3: A schematic representation of the optimal (broad profiles with moderate gradients) and non-optimal (narrow profiles with steep gradients) ITB profiles.

momentum transport channels, on DIII-D [71, 72], JET [73] and JT-60U [22]. However, there is also a number of cases where one or two transport channels exhibit an ITB while the other ones do not. Sometimes only T_i has an ITB, sometimes T_e and n_e show clear ITBs while the ITB in T_i appears only weak. This phenomenon is not fully understood, but it is probable that the heating scheme, whether it is dominantly ion or electron heating, plays an important role. In addition to this, different transport channels are affected by different micro-turbulence and because the turbulence stabilisation mechanisms become active in different plasma conditions, it is possible that ITBs appear only in some of the transport channels. In the case of simultaneous ITBs in different transport channels, the radial location and time evolution of the ITBs in those channels are similar.

It is not completely clear how the optimal ITB profile should look like. However, some general rules for the optimal ITB profile can be drawn. Firstly, it should provide the largest improvement in fusion performance that can be sustained for a long time. Secondly, good confinement is required; typically a factor of two or higher than the conventional H-mode confinement time indicates good confinement in ITB discharges. Thirdly, the plasma profiles must be stable against MHD instabilities. Fourthly, the ITB must be radially located in the region where the bootstrap current is large and well-aligned with the desired q-profile. A diagram-

matic representation of the optimal and non-optimal ITB profiles (temperature, density or pressure) is shown in Figure 2.3. The optimal ITB profiles lie at a large radius r/a, and possess moderate gradients, whereas the non-optimal ITB profiles are the opposite. A large ITB radius increases confinement. In addition, the fusion performance is improved by the increasing volume of the improved confinement region. MHD modelling indicates that the maximum stable normalised beta, $\beta_{\rm N} = \beta/(I/aB_\phi)$, can increase by 60% or more as the ITB radius and width are increased [50]. Moreover, in order to obtain a large bootstrap current fraction that is aligned well with the desired current density profile, the ITB radius should lie at $r/a \approx 0.7 - 0.8$ with moderate ITB gradients.

The most promising way to achieve long-lasting steady-state operation in tokamaks with good confinement is to have two transport barriers simultaneously — plasma that has an ITB with an H-mode (ETB) edge. This double barrier mode has provided promising results in JET [74]. Very recently, a new high performance regime, called the Quiescent Double Barrier (QDB) mode, has been found in DIII-D [50]. The QDB regime combines an ITB with a quiescent, ELM-free H-mode edge, giving rise to good confinement and a possibility to a long-pulse operation with high performance if the density can be increased and the impurity accumulation avoided.

2.3 ITB Formation Dynamics

An ITB often forms in the early phase of the discharge. In many cases, it appears during the current ramp-up phase with only a moderate heating power. These ITBs are most distinct in the electron temperature profiles. The formation of these types of ITBs in JET have been analysed in Publications 3 and 4. Another common way of obtaining ITBs is shortly after the main heating phase or high power phase has started. The formation mechanisms of these ITBs have been investigated in Publications 1, 2 and 5. After the initial formation, an ITB can expand, shrink or disappear depending on the heating power, current density profiles, MHD instabilities etc. What is worth mentioning is that the physics behind the initial formation, i.e. ITB triggering, may differ from the physics that governs the ITB dynamics and evolution later during the discharge. The physical mechanism of the ITB formation has not yet been clearly identified. There are several physical mechanisms that are believed to affect the ITB formation and dynamics of which the most common ones are analysed in detail in Secs. 2.3.1–2.3.5.

2.3.1 $\omega_{E\times B}$ Flow Velocity Shear

The importance of the radial electric field and its shear was already recognised long time ago [75, 76]. For the present, the leading candidate to explain the ITB formation and ITB dynamics in a tokamak seems to be the $E\times B$ velocity shear [77]. It is regarded as a key factor in the ITB formation in most theories [78, 79, 80] and

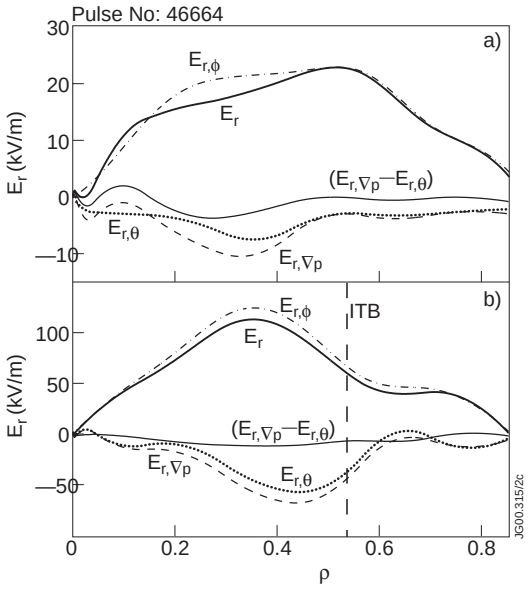

Figure 2.4: E_r and its components 0.6 s before (a) and 0.6 s after (b) the ITB formation as a function of $\rho = \sqrt{\phi/\pi B_\phi}/a_\mathrm{eff}$ with a_eff being the radius of the circle covering the same area as the elongated plasma for JET pulse No. 46664. The footpoint of the ITB is shown by the vertical dashed line in (b).

also found to be essential in most ITB experiments on different tokamaks [21, 70, 81, 82].

The radial force balance equation is written as follows:

$$E_\mathrm{r} = \frac{1}{Zen_i}\frac{\partial p_\mathrm{i}}{\partial r} - v_\theta B_\phi + v_\phi B_\theta, \tag{2.6}$$

where v_θ and v_ϕ are the poloidal and toroidal velocities and B_θ and B_ϕ the poloidal and toroidal magnetic fields, respectively, n_i is the ion density, Z is the ion charge number and e the elementary charge. Equation (2.6) indicates that there is a connection between E_r and the radial heat and particle transport through ∇p_i, toroidal rotation through v_ϕ and poloidal flow through v_θ.

The radial electric field and its different components are shown 0.6 s before the ITB formation in Figure 2.4 (a) and 0.6 s after the ITB formation in Figure 2.4 (b) for a typical 'Advanced Tokamak Scenario' JET discharge (pulse No. 46664). The contribution from the toroidal rotation (dash-dotted curve) is clearly dominant in the total E_r (thick solid), both before and after the ITB formation. The magnitude of E_r and all its components are about 5 times larger after the formation of the ITB than prior to it. The footpoint of the ITB is at $\rho \approx 0.56$ in Figure 2.4 (b). The values for E_r and its different components are found to be of the same order of magnitude and follow the same qualitative behaviour also for other JET ITB

discharges, where the ITB appears in the main heating phase.

In JET, the toroidal rotation produced mainly by the co-rotating NBI gives always a positive contribution to E_r as illustrated in Figure 2.4. However, theoretically, when exploring the interaction of the toroidal rotation with diamagnetic and poloidal rotation contributions, counter-momentum injection was predicted to lower the power threshold to form an ITB and to produce a wider ITB in Ref. [83]. Experimentally NBI counter-injection was demonstrated to be better at sustaining the ITB compared to co-injection on TFTR [70, 84]. However, balanced-injection with $v_\phi \approx 0$ turned out to be enough or even better to sustain and form an ITB on TFTR when the magnetic shear was negative in the core plasma. The advantage of balanced-injection in reversed magnetic shear plasmas has also been reported in JT-60U [81].

In a tokamak geometry, the $\omega_{E\times B}$ shearing rate is usually calculated according to the so-called Hahm-Burrell formula [85]

$$\omega_{E\times B} = \left| \frac{(RB_\theta)^2}{B} \frac{\partial}{\partial \Psi} \frac{E_r}{RB_\theta} \right|, \tag{2.7}$$

where Ψ is the poloidal flux, R the major radius and E_r calculated in Eq. (2.6). Although E_r/RB_θ is constant on a flux surface, $\omega_{E\times B}$ is not because of $(RB_\theta)^2/B$. Consequently, due to the B^{-1} dependence, the $\omega_{E\times B}$ flow shear is larger on the low field side and therefore, turbulence stabilisation occurs more easily there.

The basic theoretical picture of the $\omega_{E\times B}$ flow shear stabilisation relies either on non-linear decorrelation of turbulence [69] or linear stabilisation of unstable modes [86]. In the non-linear electrostatic model, transport (such as ITG, TEM and ETG) is caused by the correlation between the density (or temperature perturbations) and the velocity (or potential perturbations). When the $\omega_{E\times B}$ velocity shear is large enough, the turbulent eddies are distorted and as a consequence, radial transport is reduced. This reduction is due to both changes in the phase relationship between the perturbations and a decrease in the amplitude of the fluctuations. In the linear model, the presence of the $\omega_{E\times B}$ velocity shear results in enhanced damping by coupling the unstable modes to other, nearby lying stable modes, thus reducing transport. In general, turbulence quenching takes place roughly when $\omega_{E\times B}$ velocity shear is larger than the maximum growth rate of the dominant turbulence mode γ_{lin}^{max}, i.e. $\omega_{E\times B} > \gamma_{lin}^{max}$ [86].

Assuming the $\omega_{E\times B}$ shear to be the leading candidate, an ITB should form if the ITB formation threshold condition $\omega_{E\times B} > \gamma_{lin}^{max}$ is fulfilled at a certain radius at a certain time. There is also strong experimental evidence that $\omega_{E\times B}$ is comparable to γ_{lin}^{max} prior to the ITB formation and significantly exceeds it after the formation on JET [87], on DIII-D [23, 77] and on TFTR [49, 84]. Nevertheless, this does not necessarily prove the causality — which one occurs first, turbulence suppression by $\omega_{E\times B}$ shearing rate or transport reduction due to some other turbulence quenching mechanism followed by an increase in $\omega_{E\times B}$. The problem is complicated because when the temperature gradient increases, γ_{lin}^{max} increases, but so does $\omega_{E\times B}$ and usually faster. Consequently, well after the onset of the ITB, it is natural that

$\omega_{E\times B}$ exceeds significantly γ_{lin}^{max}. Nevertheless, for the present the $\omega_{E\times B}$ shearing rate seems to be the most universal mechanism to explain the ITB formation and dynamics in many experiments on many tokamaks.

2.3.2 Magnetic Shear s

There are several ways in which the magnetic shear s, i.e. derivative of the q-profile ($s \approx (r/q)(dq/dr)$), affects transport. The magnetic shear also influences the ITB formation and sustainment. With a negative magnetic shear $s < 0$, ballooning modes enter the second stable region [78, 88] with complete stability to $n = \infty$ ideal MHD ballooning modes [89]. A small or negative magnetic shear also prevents normally the sawtooth instability from becoming active ($q > 1$), thus improving the core confinement and performance. The negative magnetic shear also reduces the geodesic curvature drive of micro-instabilities, such as ITG, TEM and high-n ballooning modes [79, 89] and it also reduces magnetic stress by eliminating perturbations in B [90]. In addition, the threshold of the critical temperature gradient of the ITG turbulence increases due to negative s [91]. Furthermore, it has been also shown that $s < 0$ can reverse the toroidal precession drifts of barely trapped electrons [49]. Even some of the high-k instabilities, such as the ETG turbulence, can be stabilised by a region of the negative magnetic shear [50, 92]. Finally, in the region where $s \approx 0$, the turbulent vortices, initially linked together by toroidicity, are more easily disconnected than with large values of s, thus giving rise to improved plasma confinement [44].

In order to have a negative or small magnetic shear with all its aforementioned beneficial effects during the high performance phase of a tokamak discharge, a successful preparation phase is required to create the appropriate target q-profile. In JET, typically LHCD or sometimes ICRH is used in the preheating phase together with a fast current ramp-up to achieve the negative or small magnetic shear. This is analysed in much more details in Section 3.2 and in Publication 3. On other tokamaks, also ECRH and NBI preheating are applied in order to create the desired magnetic shear profile [38, 93, 94].

One of the key questions with the negative magnetic shear is whether it alone can trigger the ITB or it just facilitates the ITB formation while some other mechanism plays the main role. In some proposals the negative magnetic shear plays the key role [49], while other proposals state that it alone cannot form the ITB [77, 84].

In many proposals, the synergy between the effects by the negative magnetic shear and the $\omega_{E\times B}$ shearing rate is fundamental. In JET, the synergy between s and the $\omega_{E\times B}$ shearing rate is investigated in Figure 2.5. Thirteen ITB pulses in the H-mode and three ITB pulses in the L-mode at the ITB threshold condition are illustrated. There are also three back transitions from an ITB state to an ELMy H-mode plasma included in Figure 2.5. The plasma parameter range of the analysed pulses is very wide, i.e. B_ϕ varies between 1.8–4.0 T, the input power in the range 10–30 MW and the diamagnetic energy in the range 3–12 MJ among the

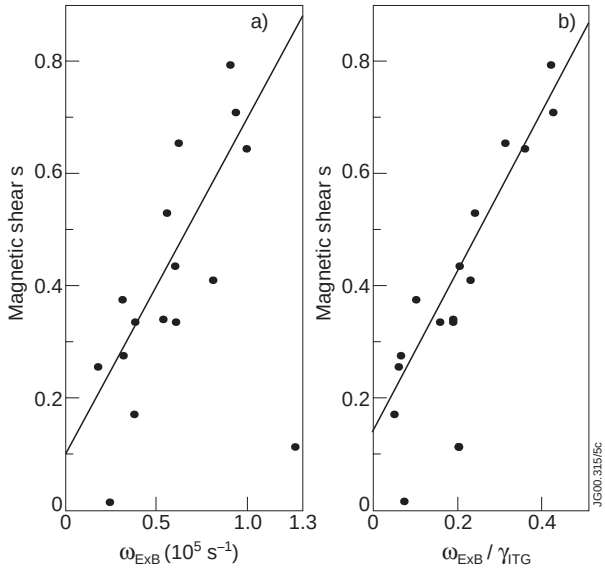

Figure 2.5: (a) Magnetic shear s as a function of $\omega_{\mathrm{E\times B}}$ at the ITB location at the ITB onset for 16 JET 'Advanced Tokamak Scenario' discharges. (b) As in (a), but $\omega_{\mathrm{E\times B}}$ shearing rate divided by the linear estimate of the ITG instability growth rate γ_{ITG}. The straight lines are the best fits calculated with the least-squares method.

investigated pulses. The magnetic shear s is calculated in an interpretative way (predicting q, taking T_{e}, T_{i} and n_{e} from experiments) by JETTO [27] transport code. In Figure 2.5, s is presented at the ITB radius at the onset of the ITB as a function of $\omega_{\mathrm{E\times B}}$ or $\omega_{\mathrm{E\times B}}/\gamma_{\mathrm{ITG}}$ with $\omega_{\mathrm{E\times B}}$ calculated from Eq. (2.7) at the same time and location.

The data points in Figure 2.5 exhibit a linear trend indicating that a linear regression is reasonable. Therefore, by applying the least-squares method to the scatter plots, a straight line in each figure can be estimated. The estimated regression line takes the form $s = 0.60\omega_{\mathrm{E\times B}} + 0.091$ ($\omega_{\mathrm{E\times B}}$ scaled by 10^5) in Figure 2.5(a) and

$$s = 1.47\omega_{\mathrm{E\times B}}/\gamma_{\mathrm{ITG}} + 0.14, \tag{2.8}$$

or by rearranging the terms

$$\omega_{\mathrm{E\times B}} = 0.68s\gamma_{\mathrm{ITG}} - 0.095\gamma_{\mathrm{ITG}}, \tag{2.9}$$

in Figure 2.5(b). The scatter among the different discharges is clearly smaller in the case where the discharges are plotted as a function of $\omega_{\mathrm{E\times B}}/\gamma_{\mathrm{ITG}}$ rather than $\omega_{\mathrm{E\times B}}$. As a consequence, this can be regarded also as an indirect indication that the ITG turbulence and the ITG turbulence suppression play a major role in the ITB formation process with these JET discharges.

There are two distinct regions in the $s - \omega_{\mathrm{E\times B}}/\gamma_{\mathrm{ITG}}$ space, separated by the straight

line from Eq. (2.8) in Figure 2.5(b). The ITB formation threshold condition is interpreted as follows: when and where $\omega_{\mathrm{E\times B}} > 0.68 s\gamma_{\mathrm{ITG}} - 0.095\gamma_{\mathrm{ITG}}$ is fulfilled, an ITB does exist whereas when and where $\omega_{\mathrm{E\times B}} < 0.68 s\gamma_{\mathrm{ITG}} - 0.095\gamma_{\mathrm{ITG}}$, an ITB does not exist. The ITB forms or collapses, depending on the direction, when the straight line given by Eq. (2.8) is crossed. The same rule is valid for all discharges in a wide range of parameters B_ϕ, P_{in} and W_{dia} [95].

The empirical threshold condition found for the ITB formation provides the first clear indication of the strong correlation between s and $\omega_{\mathrm{E\times B}}$ at the ITB transition in JET. The physics interpretation of the ITB formation in the s–$\omega_{\mathrm{E\times B}}/\gamma_{\mathrm{ITG}}$ space could be the following: the $\omega_{\mathrm{E\times B}}$ flow shear must be large enough to tear apart the turbulent eddies thus decreasing the growth rate of the long wave length ITG turbulence (γ_{ITG}) while at the same time the small (or negative) magnetic shear s helps to disconnect the turbulent vortices (e.g. ballooning modes) initially linked together by toroidicity. Another point worth mentioning is the intercept term in $s = 1.47\omega_{\mathrm{E\times B}}/\gamma_{\mathrm{ITG}} + 0.14$. A positive intercept implies that a negative or zero magnetic shear should be a sufficient condition for an ITB to exist in JET. Recent results from the previous JET experimental campaigns with LHCD preheating, considered thoroughly in Publications 3 and 4, support the idea. Using only LHCD in the preheating phase, the discharge has a very clear ITB in the electron transport channel and the magnetic shear is negative while the $\omega_{\mathrm{E\times B}}$ shearing rate and the Shafranov shift are very small, almost negligible. The above result would suggest that the negative magnetic shear alone would be a sufficient condition to form an ITB (at least in the electron transport channel in JET). In addition, in some experiments the footpoint of the ITB has been also found to follow the q_{min}-surface in JET [74]. Similar results of the special role of the negative magnetic shear has been reported from other tokamaks [96, 97]. However, there is also some evidence from other tokamaks that may contradict the aforementioned statement [70, 77].

2.3.3 Integers and Rationals of the q-profile

There is evidence on JET [98], RTP [99], JT-60U [15] and DIII-D [23] that integer and possibly also rational surfaces of the q-profile affect ITB triggering and in some cases may also have an influence on the later time evolution of the ITB. In JET, an ITB is often formed when the $q = 2$ surface appears in the core region. In addition, in many cases the footpoint of the ITB seems to follow the outward propagation of the $q = 2$ surface.

One of the proposed ideas behind the ITB triggering by an integer q surface is a link between the MHD activity on the integer q surface and the MHD activity at the edge [98]. This coupling of the magnetic perturbations with different poloidal mode numbers results via toroidicity and via the shaping of the flux surfaces [100]. The strong toroidal coupling of the external ($n = 1$) kink mode at $q_{\mathrm{edge}} = 5$ or $q_{\mathrm{edge}} = 4$ to the $q = 2$ or $q = 3$ surface in the core indicates the potential for modifying transport. The modified enhanced transport at the q integer island ($n = 1$ and $m = 2$ or $m = 3$) can locally increase or decrease the pressure and toroidal rotation

at adjacent points around the integer q surface. Therefore, the integer q surface can act as a trigger for an ITB although the actual turbulence suppression occurs via the increased $\omega_{\mathrm{E}\times\mathrm{B}}$ shearing rate. Another explanation relies on the density of the rational q surfaces; near a simple rational q surface, there are less low order rational resonant surfaces [44]. This idea works very well in the turbulence simulations. Other experimental and theoretical studies to explain the ITB formation due to the integer and rational surfaces in the q-profile have suggested different mechanisms. They rely either on a local reduction in transport associated with low order rational q surfaces or on some other topological modifications of the flux surface structure resulting from the internal MHD occurring at the rational q surfaces [101].

2.3.4 Shafranov Shift

The Shafranov shift Δ is a displacement of the magnetic axis (and flux surfaces) due to pressure and current density profiles with respect to the magnetic axis in the vacuum field. The flux surfaces in a plasma are more densely populated on the outer mid-plane and less densely on the inner mid-plane than those in the vacuum field without the plasma. The Shafranov shift has a twofold effect on the ITB formation. Firstly, it enhances the $\omega_{\mathrm{E}\times\mathrm{B}}$ shearing rate on the low field side on the outer mid-plane. This originates from Eq. (2.7); the Shafranov shift compresses the flux surfaces closer to each other on the outer midplane and thus, E_{r} is larger because the potential is constant on a flux surface. This results further in larger $\omega_{\mathrm{E}\times\mathrm{B}}$ shearing rates. Secondly, the Shafranov shift can directly affect the growth rate of the micro-turbulence, for example the growth rate of the TEM and ETG reduces significantly with a large Shafranov shift [49, 92].

The effect of the Shafranov shift on the turbulence suppression and on the ITB formation via the increased $\omega_{\mathrm{E}\times\mathrm{B}}$ shearing rate has been investigated in Publication 1. The local increase in the $\omega_{\mathrm{E}\times\mathrm{B}}$ shearing rate on the outer mid-plane as compared with the inner mid-plane was found to be very small for typical JET 'Advanced Tokamak Scenario' ITB pulses. However, although the effect of the Shafranov shift on the ITB formation via the increased $\omega_{\mathrm{E}\times\mathrm{B}}$ shearing rate may be small (at least in JET), its effect on the instability growth rate has been reported to be of great importance on TFTR [49]. The stabilisation mechanism is based on the favourable precession of the trapped electrons due to the large Shafranov shift. Transport by the TEM can be decreased significantly and even suppressed completely in the case of a large Shafranov shift. This stabilisation effect is enhanced by the small or negative magnetic shear.

The Shafranov shift stabilisation is a positive feedback mechanism — a larger Shafravov shift leads to reduced transport and steeper pressure gradient which then, in principle, can lead to even larger Shafranov shift and in turn, steeper pressure gradient. As a consequence, the Shafranov shift could be a possible trigger for the sudden transition to an ITB. Another practical issue with turbulence stabilisation by the Shafranov shift is that it has more favourable scaling to reactors than for example the $\omega_{\mathrm{E}\times\mathrm{B}}$ shearing rate because it is less dependent on the machine size.

2.3.5 Density Gradient

Certain drift waves in tokamaks, such as the ITG and the ETG, have the property that they become unstable when the temperature gradient exceeds a critical value, as already discussed in Section 2.1.1. This critical temperature gradient threshold, like the critical temperature length for the ITG $L_{T_i}^{crit}$, depends on the density gradient. Accordingly, an increase in the density gradient may stabilise the ITG or the ETG and thus lead to a bifurcation to a reduced transport state [78, 102]. Therefore, a local particle source can act as a trigger mechanism to the ITB formation. With a moderate or steep density gradient, equation (2.1) in Section 2.1.1, which is the simple approximation of the critical temperature gradient of the ITG with a flat density profile, is not valid any longer. On the other hand, even if the ITG and the ETG may be quenched by the density gradient, the TEM may be destabilised by the density gradient. Thus, anomalous transport can be suppressed completely with the density gradient mechanism only in the plasma centre and in a highly collisional edge region where trapped particles are absent.

The role of the density gradient in the ITB formation in JET is analysed in Publication 2. The simulation results indicate that indeed, the density gradient can form the ITB, independently of the $\omega_{E\times B}$ shearing rate stabilisation. The onset of the ITB is based on the suppression of the ITG turbulence by the large density gradient inside $r/a \approx 0.5$. In general, the ITG turbulence is believed to be the main source of the anomalous transport in the core region of the JET ITB plasmas and as a consequence, the turbulence suppression by the density gradient mechanism should be taken into account.

2.3.6 Interplay of the Different ITB Formation Mechanisms

As already shown in Section 2.3.2, it is not necessarily only one mechanism at a time that triggers and governs the dynamics of the ITB. Rather, it is probable that at least two of them interact with each other so that the micro-turbulence is suppressed, transport reduced and an ITB can form. Identification and evaluation of the relative importance of the different mechanisms are difficult since various types of micro-instabilities affect different transport channels and furthermore, various types of micro-instabilities are suppressed by different stabilisation mechanisms. It is also difficult to diagnose the contribution from the different stabilisation mechanisms since they are not independent of each other. For example, raising the density increases the Shafranov shift and density gradient and increases or decreases, depending on the direction of the toroidal rotation, the $\omega_{E\times B}$ shearing rate. Similarly, raising the temperature affects both the $\omega_{E\times B}$ shear and the Shafranov shift. The aforementioned complicated interaction among the different transport mechanisms affecting different transport channels, together with the stabilisation mechanisms, is illustrated in Figure 2.6.

It is important to note in Figure 2.6 that even if it seems to be possible to decrease or suppress the ITG with all turbulence stabilisation mechanisms, it can be still

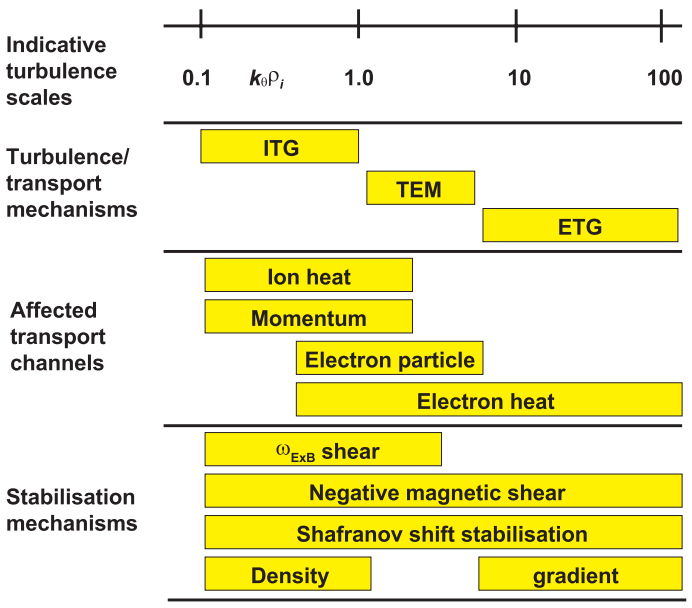

Figure 2.6: An outline summary of different transport mechanisms, how they affect different transport channels and how they can be stabilised.

regarded as the worst instability. This is due to the fact when the ITG is unstable, it also the predominant instability. Using the simple mixing length estimation, i.e. $\chi \sim \gamma / k_\theta^2$, the ITG gives the largest transport because of the longest wavelength although the growth rate γ of the ETG is much larger. As a consequence, the $\omega_{\mathrm{E}\times\mathrm{B}}$ shearing rate could be still the main turbulence stabilisation mechanism because it can efficiently suppress the ITG. The role of the rational q-surfaces is not illustrated in Figure 2.6 because it most probably affects transport indirectly via the other mechanisms, like increasing locally the $\omega_{\mathrm{E}\times\mathrm{B}}$ flow shear or the density gradient.

It might be expected that it is easiest to obtain ITBs in the ion heat and momentum transport channels, somewhat harder in the particle transport channel, and hardest in the electron heat channel. This tendency is consistent with observations on DIII-D [50]. In JET, with strong LHCD during the current ramp-up in the preheating phase, a clear ITB appears in the electron heat channel. However, no ITB in the ion heat or electron particle transport channels can be observed. Therefore, an interesting question remains whether this is just a measurement problem due to the low ion temperature and electron density or whether there is a contradiction with the results from DIII-D.

2.4 Numerical Codes and Transport Models

In this thesis, all the transport simulations have been performed with the JETTO transport code [27]. JETTO is a one and a half dimensional general transport code solving the time-dependent plasma diffusion equations averaged over the magnetic flux surfaces. In addition to solving the transport equations, JETTO has an internal equilibrium solver, several heating and current drive packages, calculation of the radial electric field, calculation of the fusion power and so on. Furthermore, JETTO transport code has several transport models, both empirical and theory-based ones.

2.4.1 JETTO Transport Code

The transport equations for the particle transport channel (Eq. (2.10)), for the electron heat transport channel (Eq. (2.11)), for the ion heat transport channel (Eq. (2.12)) and for the poloidal magnetic flux (current density) (Eq. (2.13)) can be written as follows:

$$\frac{1}{V'}\frac{\partial}{\partial t}(V' n_j) + \frac{1}{V'}\frac{\partial}{\partial \rho}(V'\langle(\nabla\rho)^2\rangle\Gamma_j) = \langle S_{\mathrm{n}_j}\rangle, \qquad j = 1, ..., n_H \quad (n_H < 3) \tag{2.10}$$

$$\frac{3}{2}(V')^{-5/3}\frac{\partial}{\partial t}\left[(V')^{5/3} n_{\mathrm{e}} T_{\mathrm{e}}\right] + \frac{1}{V\prime}\frac{\partial}{\partial \rho}\left\{V'\langle(\nabla\rho)^2\rangle\left[q_{\mathrm{e}} + \frac{5}{2}T_{\mathrm{e}}\Gamma_{\mathrm{e}}\right]\right\} = \langle P_{\mathrm{e}}\rangle \tag{2.11}$$

$$\frac{3}{2}(V')^{-5/3}\frac{\partial}{\partial t}\left[(V')^{5/3}\sum_{j=1}^{n_H} n_j T_{\mathrm{i}}\right] + \frac{1}{V'}\frac{\partial}{\partial \rho}\left\{V'\langle(\nabla\rho)^2\rangle\left[\sum_{j=1}^{n_H} q_j + \frac{5}{2}T_{\mathrm{i}}\Gamma_j\right]\right\} = \langle P_{\mathrm{i}}\rangle \tag{2.12}$$

$$\frac{\partial\psi}{\partial t} - \frac{A\eta_{||}}{\rho\mu_0}\frac{\partial}{\partial\rho}(K\frac{\partial\psi}{\partial\rho}) + \frac{V'\eta_{||}}{2\pi\rho}(j_{\mathrm{bs}} + j_{\mathrm{cd}}) = 0, \tag{2.13}$$

where the toroidal flux surface label ρ is defined as $\rho = \sqrt{\phi/\pi B_\phi}$ with ϕ being the toroidal flux and ψ is the poloidal flux. V is the volume and V' denotes the differentiation with respect to ρ. The brackets $\langle\rangle$ denotes the flux surface average, A and K are geometrical factors and μ the permeability of the vacuum. The electrical resistivity $\eta_{||}$ is a slightly modified version of Eq. (2.5). The particle and heat fluxes are denoted with Γ_j and q_j, respectively. S_{n_j}, P_{e} and P_{i} represent sources and sinks due to auxiliary heating and fuelling, energy exchange between different species, charge exchange losses, radiation, losses due to background neutrals and ionisation etc. j_{bs} and j_{cd} are the bootstrap current and externally driven current, respectively. The contribution from the transport models enter the equations (2.10)–(2.12) into the terms Γ_j and q_j. These terms are calculated from the transport matrix in Eq. (1.5) with the diffusion coefficients given by the transport models. In addition, there is a momentum balance equation in order to follow the time evolution of the toroidal rotation in JETTO.

The transport equations, i.e. the energy, particle and current balance equations, (2.10)–(2.13) form a complex integro-differential system. As a consequence, an

appropriate set of initial and boundary conditions is required in order to predict the time evolution of the simulated unknown quantities, such as n_e, T_e, T_i and B_θ. In JETTO, the initial profiles of all the unknown quantities that are to be modelled are read from an external file at the first time step. The initial profiles are constructed either from the experimental data or from some prescribed formula. For the initial condition in the poloidal magnetic field equation, an initial q-profile from EFIT [103] is used. EFIT is an equilibrium reconstruction code which calculates, among other, the equilibrium, the flux surfaces and the q-profile. The boundary conditions are needed both in the centre and at the separatrix. In the centre, the boundary condition of all the unknown quantities takes the form $\partial u/\partial \rho = 0$, where u is the unknown quantity to be modelled. At the separatrix, the boundary conditions are employed with the aid of time polygons, indicating the time evolution of the unknown quantity at the edge. Typically, experimental values at the plasma edge are imposed in JETTO. For example in JET, when the H-mode appears, the boundary value for T_e or T_i rises from about 300 eV up to 1.2 keV within some tens of milliseconds. The boundary condition for the poloidal magnetic field equation is the total plasma current. In addition, the value of Z_{eff} is needed in the simulations and normally, the experimentally measured value is used.

There are several other numerical modules than the transport equation solver coupled to JETTO. Several heating and current drive packages, neutral particle calculation package, fusion power calculation package etc. are implemented and coupled to JETTO. One of the most fundamental ones is the equilibrium package ESCO. ESCO takes the pressure and current density profile as input from JETTO and then solves the Grad-Schlüter-Shafranov equation in order to calculate the equilibrium and flux surfaces. The plasma boundary is normally taken from the experiment, i.e. from the EFIT output. Another way to introduce the equilibrium in JETTO is to use directly the EFIT equilibrium. The equilibrium is always calculated at the beginning of the JETTO transport simulation and can be recalculated later during the transport calculation as many times as needed.

The power deposition and current density profiles of LHCD in JETTO are calculated with the Fast Ray Tracing Code (FRTC) [32], which is coupled to JETTO. FRTC includes a fast ray-tracing package and the calculation of the power deposition and current density profiles by iteration between the evaluation of the quasi-linear diffusion coefficient and a 1D Fokker-Planck equation for the electron distribution function. A comprehensive study of its properties has been done in Publication 6. Since FRTC is coupled to JETTO, self-consistent simulations between transport and Lower Hybrid (LH) power and current calculation can be achieved. The coupled JETTO/FRTC code has been validated and tested in Publication 5.

In order to calculate the NBI power deposition and current density profiles in JETTO, the NBI code PENCIL [34] is used. PENCIL is also coupled to JETTO. It solves a simplified Fokker-Planck equation that is used to describe the fast ion dynamics. Fast ion self-collisions and the effects of the toroidal electric field on the fast ion dynamics are neglected. The resulting bounce averaged Fokker-Planck equation is then solved using an eigenfunction expansion in the pitch angle variable. On-axis/off-axis power deposition profiles are produced by an appropriate selection

between the normal and tangential PINIs, normal PINIs producing NBI power perpendicular to the toroidal direction (on-axis power deposition) and tangential PINIs at angles smaller than 90° with respect to the toroidal direction (off-axis power deposition).

The calculation of ECRH and ECCD is done with the 3D code ECWGB [33]. ECWGB calculates the propagation and absorption of the electron cyclotron waves injected as collimated microwave gaussian beams in toroidal geometry. The ECRH power absorbed and the ECCD current generated by highly collimated gaussian beams are evaluated using the equilibrium from JETTO and the relativistic treatment of the wave propagation and driven current. In addition, the effects of the trapped particles are taken into account. The toroidal and poloidal angles of the ray launching direction can be steered to change radially the location of the power absorption and the amount of the generated current.

The only heating method that is not dealt with in a self-consistent way in JETTO is ICRH. The power deposition profiles for electrons and ions are calculated with the ICRH code PION [104]. The PION code calculates the Ion Cyclotron Resonance Frequency (ICRF) heating power deposition profiles by taking into account the time evolution of the distribution functions of the resonating ions. In the 'Advanced Tokamak Scenario' discharges on JET, typically the hydrogen minority scheme (hydrogen concentration typically 2–4 %) is applied with frequencies in the range of 42–51 MHz to obtain on-axis and off-axis power deposition. The driven ICRH current is negligible for this ICRH scheme.

2.4.2 Transport Models in JETTO

There are three different transport models implemented in JETTO to predict the heat and particle transport. They are called the Bohm/GyroBohm model [25] which is semi-empirical, the Weiland model [28] and the Multi-Mode Model (MMM) [105] which are both theory-based transport models. Moreover, JETTO has a sawtooth model, a model for ELMs physics and an ablation model for pellet injection which are not considered in this thesis.

The Bohm/GyroBohm semi-empirical model has been tested against several different plasma discharges from DIII-D, TFTR, JT-60U, ASDEX-U, START and JET in the L-mode and against many different plasma shots performed on JET in the H-mode [20, 26, 25]. This transport model has been used in Publications 1–5. The set of the heat and particle transport coefficients in the Bohm/GyroBohm model

can be written in the following form:

$$\chi_{\rm e} = 1.0\chi_{\rm gB} + 2.0\chi_{\rm B} + \chi_{\rm neo-al} \tag{2.14}$$

$$\chi_{\rm i} = 0.5\chi_{\rm gB} + 4.0\chi_{\rm B} + \chi_{\rm i}^{\rm neo} \tag{2.15}$$

$$D = [0.3 + 0.7\rho]\frac{\chi_{\rm e}\chi_{\rm i}}{\chi_{\rm e} + \chi_{\rm i}}, \tag{2.16}$$

$$\text{where} \quad \chi_{\rm gB} = 5 \times 10^{-6}\sqrt{T_{\rm e}}\left|\frac{\nabla T_{\rm e}}{B_\phi^2}\right| \tag{2.17}$$

$$\chi_{\rm B} = \chi_{\rm B_0} \times \Theta(-0.14 + s - 1.47\omega_{\rm E\times B}/\gamma_{\rm ITG}) \tag{2.18}$$

$$\text{with} \quad \chi_{\rm B_0} = 4 \times 10^{-5} R\left|\frac{\nabla(n_{\rm e}T_{\rm e})}{n_{\rm e}B_\phi}\right| q^2 \times \left(\frac{T_{\rm e}(0.8\rho_{\rm max}) - T_{\rm e}(\rho_{\rm max})}{T_{\rm e}(\rho_{\rm max})}\right) \tag{2.19}$$

$$\text{and} \quad \chi_{\rm neo-al} = \frac{c^2 v_{\rm th}}{\omega_{\rm pe}^2 qR}\epsilon. \tag{2.20}$$

In Eqs. (2.17)–(2.20), $T_{\rm e}$ and $T_{\rm i}$ are the electron and the ion temperatures, respectively, $n_{\rm e}$ is the electron density, B_ϕ the toroidal magnetic field, c the speed of light, $v_{\rm th}$ and $\omega_{\rm pe}$ are the electron thermal velocity and plasma frequency as well as R is the major radius and ϵ the inverse aspect ratio. The non-locality in the Bohm transport appears in the last term where ρ is the flux surface label defined by $\rho = \sqrt{\Phi/\pi B_\phi}/a_{\rm eff}$ with $a_{\rm eff}$ being the radius of the circle covering the same area as the elongated plasma. Φ is the toroidal magnetic flux and $\rho_{\rm max}$ is the value of ρ at the separatrix in the L-mode and on top of the barrier in the H-mode. All the units appearing in Eqs. (2.14)–(2.20) are in SI units except $T_{\rm i}$ and $T_{\rm e}$ whose unit is eV. $\chi_{\rm i}^{\rm neo}$ is the neo-classical term for the ion heat transport [12]. $\chi_{\rm neo-al}$ term represents transport arising from the ETG turbulence and has the similar form to one proposed already long time ago by Ohkawa [106]. Recently, this form of ETG transport has been supported by non-linear gyro-kinetic calculations and found to match experiments reasonably well [92].

The Θ-function multiplying the Bohm transport in Eq. (2.18) is the Heaviside step function. The controlling parameter inside its argument is the empirical ITB formation threshold condition that was found in Publication 1 and presented in Eq. (2.8). When the argument x in the step function $x = -0.14+s-1.47\omega_{\rm E\times B}/\gamma_{\rm ITG}$ changes its sign, the ITB either forms $[\Theta(x < 0) = 0]$ or collapses $[\Theta(x > 0) = 1]$ in the model. $\omega_{\rm E\times B}$ stands for the flow shearing rate defined in Eq. (2.7) and $\gamma_{\rm ITG}$ is an approximation for the linear growth rate of the ITG instability, defined as $\gamma_{\rm ITG} = v_{\rm th,i}/R$ with $v_{\rm th,i}$ being the ion thermal velocity. The toroidal velocity is calculated from the momentum balance equation using the torque from the neutral beam injection as the source term. The anomalous toroidal viscosity coefficient is assumed to be equal to the ion heat transport coefficient given in Eq. (2.15). The poloidal rotation is assumed to be neo-classical.

The other core transport model used in this thesis (Publication 2) is based on the fluid theory where the fluid equations are solved for each plasma species. Then, the fluid equations are linearized, with taking into account the magnetic drifts for each plasma species. The eigenvalues and eigenvectors from these equations are

computed for a given Fourier harmonic of the perturbed variables. Using the quasi-linear approximation, the saturation level is approximated by taking the mixing length estimate and balancing the linear growth. Then, the heat and particle fluxes can be calculated. The diffusion coefficients are calculated by taking the finite difference derivatives of the fluxes with respect to the temperature and density gradients. The model does not calculate the entire spectrum of the turbulence with respect to poloidal mode number k_θ, but a value of $k_\theta \rho_s = 0.316$ representing the middle of the spectrum is used (ρ_s is the larmor radius). This assumption produces a GyroBohm transport model. In this thesis, we call this transport model as the Weiland model [28, 29, 30, 31, 43]. The Weiland model includes electromagnetic effects as well as the effects of electron-ion collisions, impurities and fast ions.

The transport coefficients in JETTO with the implemented Weiland model have the following form:

$$\chi_e = \chi_{e,weil} + \chi_{neo-al}, \tag{2.21}$$

$$\chi_i = \chi_{i,weil} + \chi_i^{neo}, \tag{2.22}$$

$$D = D_{weil}, \tag{2.23}$$

where $\chi_{e,weil}$, $\chi_{i,weil}$ and D_{weil} are the transport coefficients from the ITG and TEM micro-turbulence, calculated by the Weiland model. Both the diagonal, off-diagonal and convective terms in the transport matrix (Eq. (1.5)) are calculated. There are two important issues worth mentioning in the present implementation of the Weiland model in JETTO. Firstly, there is no numerical fitting parameter in the present version and secondly, there is no additional term giving some extra transport in the edge region as in most of the other transport codes where the Weiland model has been implemented. Therefore, the ITB formation and the overall transport predictions can be regarded as rather theory-based predictions.

Chapter 3

Modelling of ITB Dynamics and Current Profile Evolution in JET

All the main results from the numerical modelling of the 'Advanced Tokamak Scenarios' performed during this thesis are presented in this Chapter. The predictive simulations of the 'Advanced Tokamak Scenarios' in this thesis concentrate on two subtopics. The first topic in Section 3.1 focuses more on predictive transport modelling of the ITB dynamics in JET (Publications 1, 2 and 5) whereas the second one in Section 3.2 concentrates on issues related to the modelling of the current density profile (or q-profile) evolution with respect to different heating and current drive scenarios in JET (Publications 3, 4 and 5).

3.1 Predictive Modelling of Discharges with Internal Transport Barriers

The predictive accuracy of most of the one-dimensional transport models in the ELMy H-mode scenarios is of the order of 20% [35]. As a consequence, when modelling the 'Advanced Tokamak Scenario' discharges, a better agreement between the experimental and predicted ITB dynamics can hardly be expected. In this thesis, the predictive simulations are defined to be simulations where the ion and electron temperatures, the density and usually also the toroidal rotation as well as the current density evolution are predicted by a transport model. Since the ITB formation and dynamics is not yet understood, no fully theory-based model based on first- principles and without any fitting parameters for explaining the physics of the ITBs exists for the moment. However, phenomenological transport models

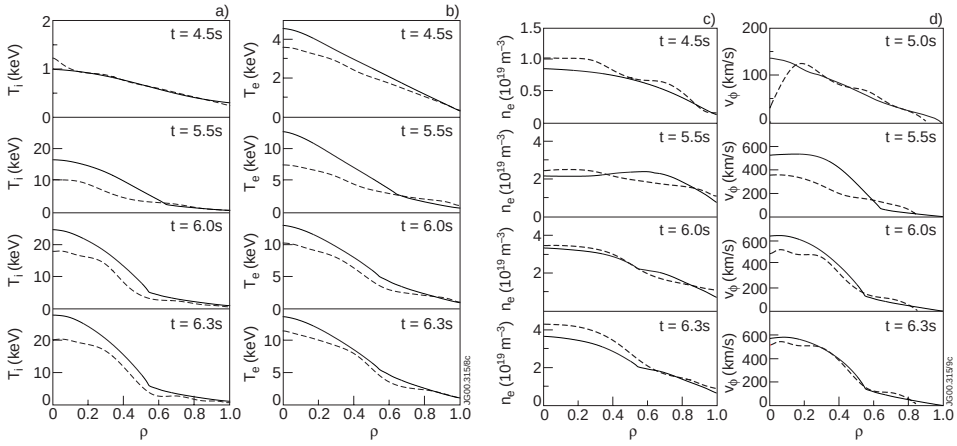

Figure 3.1: The ion (a) and the electron (b) temperatures as well as the density (c) and toroidal velocity profiles (d) at $t = 4.5$ s, $t = 5.5$ s, $t = 6.0$ s and $t = 6.3$ s. Dashed curves correspond to the experiment (Pulse No. 46664) and solid curves are calculated by the transport model.

have been successful at reproducing qualitative and numerous quantitative features in the ITB dynamics. The goodness of the empirical ITB formation threshold condition presented in Eq. (2.8) is tested in Section 3.1.1 and the applicability of the Weiland model to predict the behaviour of the ITB plasmas in Section 3.1.2. Results from the ITB modelling performed in this thesis are compared with predictions calculated by other ITB models in Section 3.1.3.

3.1.1 ITB Formation with the Empirical Transport Model

In order to demonstrate how the empirical transport model, together with the found threshold condition for the ITB formation, is able to predict the profiles of the temperatures, density and toroidal rotation, the simulation results of the JET 'Advanced Tokamak Scenario' pulse No. 46664 are illustrated in Figure 3.1. The magnetic field and the plasma current are $B_\phi = 3.4$ T, $I_\mathrm{p} = 3.4$ MA (peak). The simulation starts at $t = 3.0$ s while the NBI and ICRH heating begins at $t = 4.6$ s. The discharge ends up with a disruption due to the emergence of a pressure driven kink instability at $t = 6.5$ s. This pulse was selected here because it has a very strong and clear ITB formation, both in time and space, and also the time evolution of the ITB can be tracked with small experimental errors. The ITB forms at $t = 5.6$ s and the H-mode appears earlier at $t = 5.1$ s. The q-profile is monotonic but flat with the magnetic shear being almost zero over a large region in the plasma core. The q-profile calculated by JETTO is in good agreement with the q-profile reconstructed by EFIT.

Table 3.1: The prediction uncertainties of the transport simulations.

JET Pulse Number	47843	49196	47170	46664	47413	46998
B_ϕ [T]	1.8	2.5	3.0	3.4	3.4	4.0
$P_{\rm in}$ [MW]	14	16	25	22	30	20
$W_{\rm dia}$ [MJ]	3	4	11	10	12	6
Experimental ITB onset time [s]	2.1	4.4	5.6	5.6	6.2	6.3
Simulated ITB onset time [s]	2.3	4.1	5.4	5.2	6.1	5.7
Exper. ITB width at onset [r/a]	0.42	0.28	0.50	0.44	0.53	0.32
Simul. ITB width at onset [r/a]	0.44	0.28	0.42	0.48	0.42	0.38
Experimental ITB location [r/a]	0.30	0.29	0.54	0.56	0.58	0.33
Simulated ITB location [r/a]	0.41	0.40	0.57	0.57	0.52	0.34
$\sigma_{\rm T_i}$ [%]	23	17	18	20	17	29
$\sigma_{\rm T_e}$ [%]	24	9	7	16	15	12
$\sigma_{\rm n_e}$ [%]	13	11	6	6	7	17
$\sigma_{\rm v_\phi}$ [%]	$--$	9	16	10	19	17

As is seen, the simulation clearly predicts the existence of the ITB. However, the temperatures, in particular the ion temperature, are overestimated by the transport model. This is mainly due to the ITB threshold condition that triggers the ITB by 0.4 s too early at $t = 5.2$ s for this discharge. This is illustrated by the second time slices at $t = 5.5$ s in Figure 3.1 (ITB does not yet exist in the experiment). The last two time slices describe the highest performance phase where the ITB also exists in the experiment. The model overestimates the location of the barrier by 5–7 cm at $t = 6.0$ s, but later before the disruption at $t = 6.3$ s, the experimental location of the ITB is in agreement with the prediction. The simulated and experimental density and toroidal velocity profiles are presented at the same instants as the temperatures in Figure 3.1(c) and (d).

A comprehensive predictive analysis (in Publication 1) includes several JET 'Advanced Tokamak Scenario' discharges from a wide plasma parameter range of $B_\phi = 1.8$–4.0 T, $P_{\rm in} = 14$–30 MW and $W_{\rm dia} = 3$–12 MJ. The transport model with the ITB threshold condition is identical for all the analysed discharges. The statistics shown in Table 3.1 indicates that the temperature profiles $T_{\rm i}$ and $T_{\rm e}$ generally match the experimental data with prediction errors of the order of 10–25 %, thus being roughly of the same order as the experimental measurement errors that are within 5–20 % in JET. The accuracy in $n_{\rm e}$ and v_ϕ profiles is even better, typically the time averaged prediction errors are in the range of 10–20 %. The pulse No. 46664 that was illustrated in Figure 3.1 turned out to have the poorest agreement with the experiment among the chosen discharges. There is also a trend that the model triggers the ITB too early (pulse No. 47843 is an exception) whereas no similar trend can be observed in the location of the ITB. Furthermore, the magnitude of the overall simulation error does not seem to depend on the magnetic field nor on any other global plasma parameter.

3.1.2 ITB Formation according to the Theory-Based Weiland Transport Model

In the ITB formation, the Weiland model takes into account the $\omega_{\mathrm{E\times B}}$ shearing rate, the magnetic shear and the density gradient stabilisation mechanisms. The following issues can be concluded when the Weiland model is applied to the same pulse as illustrated in Figure 3.1. Firstly, the Weiland model produces an ITB. The onset time of the ITB is reproduced within 0.1 s accuracy, thus more accurately than the Bohm/GyroBohm model does. On the other hand, the location of the ITB is clearly better reproduced with the Bohm/GyroBohm model than with the Weiland model. The Weiland model overestimates the density and the electron temperature, in particular in the L-mode. The agreement in the location of the ITB and in the temperature profiles between the experimental and modelling results would be better if the density were taken from the experiment rather than modelled. However, this would reduce the self-consistency and make the transport model comparison more biased.

The next obvious question is that because the Weiland model produces an ITB, what is the dominating formation mechanism. The analysis of the effect of the $\omega_{\mathrm{E\times B}}$ shearing rate on the ITB formation and temperature profiles is done in Publication 2. Surprisingly, practically no difference between the case with the actual shearing rate, where the shearing rate is calculated from [85], and the case with zero shearing rate is found. However, both cases exhibit a clearly visible ITB. Therefore, the importance of the $\omega_{\mathrm{E\times B}}$ shearing rate in the ITB formation seems to be questionable according to the Weiland model and thus, there must be something else that governs the ITB dynamics in the model.

The next study concerns the effect of the density gradient on the ITB formation. Two predictive simulations are compared, one with the actual NBI power and particle source and another one with the same NBI power but with no particle source. The results from the simulations are illustrated in Figure 3.2.

The threshold of the critical ion temperature gradient length $L_{\mathrm{T_i}}^{\mathrm{crit}}$ to turn on the ITG turbulence depends on the density gradient. Then, even with a moderate density gradient, equation (2.1) is not valid but depends on the density gradient. Therefore, having a larger density gradient allows one to have also a larger temperature gradient while simultaneously preventing the ITG micro-turbulence from becoming unstable. Consequently, a large density gradient can act as an ITB formation mechanism provided that the drive due to the TEM is small enough. Interestingly, the good confinement in the so-called Pellet Enhanced Performance (PEP) mode observed in JET 10 years ago was also explained to be due to the favourable effects provided by the large density gradient [107].

The following conclusions from Figure 3.2 can be drawn: because the density gradient is much larger with the NBI particle source (solid curves), the critical temperature gradient length $L_{T_{\mathrm{i}}}^{\mathrm{crit}}$ of having the ITG unstable is smaller. Therefore, the ITG turbulence is suppressed and as a consequence, an ITB can form. This will

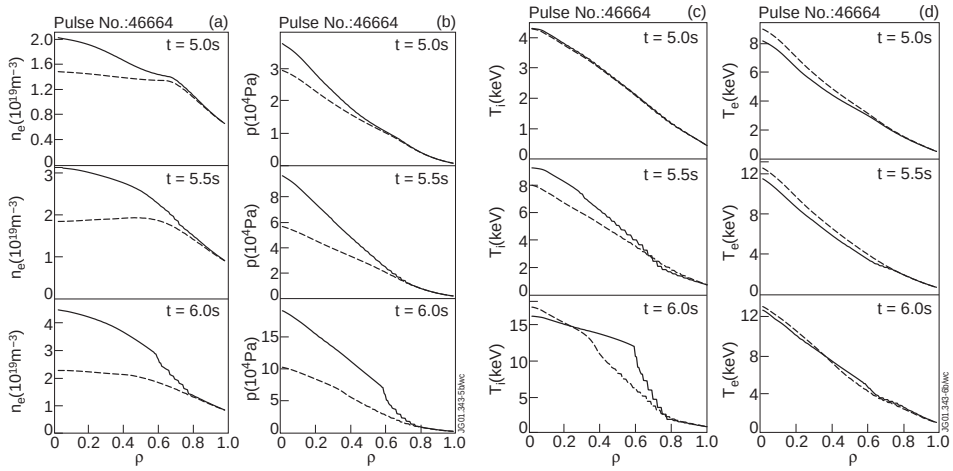

Figure 3.2: Electron density (a), pressure (b), ion temperature (c) and electron temperature (d) profiles at $t = 5.0$ s (L-mode), $t = 5.5$ s (H-mode) and $t = 6.0$ s (H-mode + ITB). The solid curve corresponds to the modelling with the NBI particle source and the dashed one without it.

then lead inevitably to significantly better confinement and larger pressure (shown in Figure 3.2(b)). As can be seen in Figure 3.2(c), the ITB clearly exists with the NBI particle source (solid curve) and is missing without the NBI particle source (dashed curve). Consequently, according to the Weiland model, the importance of the density gradient seems to dominate the effect of the $\omega_{\mathrm{E}\times\mathrm{B}}$ shearing rate in governing the dynamics of the ITB. This is quite contrary to what was found in Secs. 3.1.1 and Publication 1, i.e. where the ITB formation threshold condition was found to depend strongly on $\omega_{\mathrm{E}\times\mathrm{B}}$ and s.

3.1.3 Comparison of ITB Dynamics Calculated by Other Transport Models

The Multi-Mode Model (MMM) is a combination of theory-based transport models used to predict the temperature and density profiles in tokamaks [105]. MMM consists of the Weiland model [28, 29, 30, 31, 43] for the ITG and TEM modes, the Guzdar-Drake model for drift resistive ballooning modes [52] as well as smaller contributions from the kinetic ballooning modes and neo-classical transport. It has been found that the MMM transport model predicts temperature and density profiles that match the experimental data more closely (within 15% accuracy) than any other theory-based model currently available [105]. The formation of the ITB is interpreted as a combination of the $\omega_{\mathrm{E}\times\mathrm{B}}$ flow shear and magnetic shear mechanisms [108]. In order to match the location and timing of the ITB onset, a factor of 3–5 is required to multiply the calculated $\omega_{\mathrm{E}\times\mathrm{B}}$ flow shear for JET plasmas

whereas for DIII-D, no such a factor is needed. This large variation in the fitting factor between different tokamaks is an indication of significant uncertainties in the ITB formation mechanism in the model.

The Gyro-Landau-Fluid (GLF) transport model is developed from 3D gyro-kinetic stability calculations for the linear growth rates of the instabilities and from 3D gyro-Landau fluid simulations to determine the saturation levels [109]. It yields quasi-linear estimates of diffusivities of the particle, heat and momentum transport and includes turbulence suppression mechanisms of $\omega_{\mathrm{E}\times\mathrm{B}}$ flow shear, Shafranov shift and magnetic shear. The model can be characterised as a stiff model and, as a distinguishing feature the model includes the physics of the ETG mode. The ITB formation in the GLF model occurs normally in two stages; when the $\omega_{\mathrm{E}\times\mathrm{B}}$ flow shear approaches the maximum linear growth rate of the turbulence, the profiles begin to dither between the phase with an ITB and without it [110]. Finally, the $\omega_{\mathrm{E}\times\mathrm{B}}$ flow shear exceeds the growth rate and a clear ITB can be observed. According to the model, the $\omega_{\mathrm{E}\times\mathrm{B}}$ flow shear is the key mechanism in the ITB formation. In order to have an agreement with experiments, a multiplier 1.1 for the $\omega_{\mathrm{E}\times\mathrm{B}}$ flow shearing rate in DIII-D plasmas is needed while the same multiplier has to be 2.65 for JET plasmas. The model is able to predict the steady-state temperatures and densities within 20% accuracy.

The theory-based Current-Diffusive Ballooning Mode (CDBM) transport model is based on self-sustained turbulence of current-diffusive ballooning modes [111]. The $\omega_{\mathrm{E}\times\mathrm{B}}$ flow shear, magnetic shear and Shafranov shift are taken into account in the ITB formation. The $\omega_{\mathrm{E}\times\mathrm{B}}$ shearing rate seems to be the dominating mechanism. The CDBM also includes a model for the collapse of the ITB; if the critical pressure gradient limit is exceeded, the electron viscosity is selectively enhanced, and this results in enhanced turbulence and transport and finally, in the collapse of the ITB. Good agreement with ITB experiments on JT-60U has been achieved with CDBM, but in order to reproduce the long sustainment of the ITB, however, further improvement of the transport model is necessarily required [112].

There are also various other theory-based transport models capable of predicting the dynamics of the ITBs. One of them exhibits an oscillatory or bursty behaviour close to the ITB transition [113]. The diffusion coefficients are proportional to the density fluctuation level whose evolution is modelled separately. There is also a model, called Transport Barrier Dynamics (TBD) model, that is based on bifurcations due to the sharp radial gradients and the fast time dynamics occurring in the radial transport [114]. Another bifurcation model for the ITB formation that is based on the local fluctuation intensity of the density explains the onset of the ITB as the synergism between the $\omega_{\mathrm{E}\times\mathrm{B}}$ shearing rate and the magnetic shear [79]. The model is able to predict the favourable dependence on the temperature ratio ($T_{\mathrm{i}}/T_{\mathrm{e}}$) and on the density profile peakedness as well as the unfavourable scaling with the density. There are also semi-empirical transport models that have been used to predict the ITB evolution. The q-comb model explains the electron diffusivity as a direct function of the safety factor q [101]. Low values of χ_{e} exist at low order rational surfaces of the q-profile and on the contrary, high values of χ_{e} between them. Consequently, ITBs are formed at low order rational surfaces of

the q-profile. The model works well in RTP tokamak and it is also in good agreement with many JET ITB pulses [115]. However, the q-comb model is not able to explain the ion thermal transport or ion ITBs. Simulations of ASDEX Upgrade plasmas with ITBs have shown that the Weiland model is capable of reproducing sufficiently well the experimental results [116]. The other transport models tested on ASDEX-U, i.e. IFS/PPPL [117], CDBM and Bohm/GyroBohm transport models, tend to underestimate the central values of both T_i and T_e and often also fail to form the ITB.

To conclude this section, the accuracy of the present Bohm/GyroBohm transport model with the empirical ITB model in predicting JET 'Advanced Tokamak Scenario' discharges is at least as good as that of the other models. The extensive use of the found empirical ITB formation threshold condition during the course of this thesis gives confidence in the belief that the $\omega_{\mathrm{E}\times\mathrm{B}}$ shearing rate and the magnetic shear play the major role in governing the ITB dynamics. However, the results from the Weiland model concerning the ITB formation in JET are rather contradicting. The Weiland model is also the basis for the MMM model and in order to reproduce ITBs in JET with MMM, an additional multiplier of 3–5 for the $\omega_{\mathrm{E}\times\mathrm{B}}$ shearing rate is needed. This observation is in agreement with present results from the Weiland model, stating that the $\omega_{\mathrm{E}\times\mathrm{B}}$ shearing rate, at least without any additional multiplier like in MMM, is not enough to form an ITB in JET. One conclusion could be that the importance of the $\omega_{\mathrm{E}\times\mathrm{B}}$ flow shear has been overestimated by many transport models. Another conclusion could be that the fluid theory used in deriving the Weiland model underestimates the importance of the $\omega_{\mathrm{E}\times\mathrm{B}}$ shearing rate and possibly also the effect of a small or negative magnetic shear. However, since the MMM model can produce ITBs in TFTR and DIII-D without an additional multiplier, one could also conclude that the importance of the $\omega_{\mathrm{E}\times\mathrm{B}}$ shearing rate in governing the ITB dynamics in JET is less important than found in TFTR and DIII-D.

3.2 Simulations of the Current Profile Evolution

As it has been demonstrated in Secs. 2.3 and 3.1 as well as in Publication 1, the current density profile is a key issue in governing the formation and dynamics of the ITB. As a consequence, detailed modelling of the current or the q-profile evolution must be inherently integrated to the studies of the 'Advanced Tokamak Scenarios' and the physics of the ITBs. The behaviour of the current profile evolution can be divided into two separate phases; into the preheating or prelude phase, when the plasma current is ramped-up at low density, and into the main heating or high performance phase. In the preheating phase the current density profile can be tailored relatively easily to the desired one by means of Ohmic current ramp-up and external current drive as well as electron heating. In the main heating phase on the contrary, tailoring of the current density profile is difficult due to the large density inhibiting efficient external current drive and due to high T_e resulting in the long current diffusion time. Consequently, the current density profile, achieved

in the preheating phase, is rather tried to keep fixed than significantly modified in the high performance phase. This is very difficult since the current diffusion time although long, is not infinite, being typically of the orders of tens of seconds in JET. Thus, minimising the unwanted changes by means of the external current drive and proper alignment of the bootstrap current is the best one can do.

The current density profile evolution in the preheating phase with respect to different heating and current drive methods is studied in Section 3.2.1 (Publication 3). As a fascinating special case of this, a so-called core current hole obtained with LH heating and current drive together with a fast current ramp-up is analysed in Section 3.2.2 (Publication 4). The effect of the efficient current profile control in the main heating phase on plasma performance, fusion power and the physics of the ITB is presented in Section 3.2.3 (Publication 5).

3.2.1 Impact of Different Heating and Current Drive Methods on the Early q-profile Evolution

The current profile evolution during the preheating phase in JET has been studied in a systematic way with the JETTO transport code. The following preheating methods are considered and compared: Ohmic, LHCD, on-axis and off-axis ICRH, on-axis and off-axis NBI as well as ECCD. The basic principle used in this study is that the power deposition and external current density profiles are calculated in a self-consistent way (except ICRH). Consequently, the codes to calculate the power deposition profiles are coupled to JETTO to allow a self-consistent simulation cycle between the transport and power deposition (plus current density) calculation with time. The start time of the simulation is at $t = 1.0$ s. In the simulations, the main plasma parameters ($B_\phi = 3.4$ T, $I_\mathrm{p} = 0.7$ MA at $t = 1.0$ s and $I_\mathrm{p} = 2.3$ MA at $t = 5.0$ s) as well as the initial and boundary conditions for T_e are taken from JET 'Advanced Tokamak Scenario' discharge No. 51897. The initial q-profile is from EFIT. The external heating power is 5 MW except in the case of LHCD when the power is 3 MW. Thus, the simulations are identical except in terms of the heating and current drive methods.

The q-profiles at $t = 4.0$ s and $t = 5.0$ s produced by the different preheating methods are compared in Figure 3.3. On the basis of the modelling calculations, the preheating methods can be divided into three categories in terms of the created q-profile at the end of the preheating phase [118]. LHCD and ECCD form category 1 as being the only methods that can produce deeply reversed q-profiles. Quantitatively the q-profiles produced by LHCD and ECCD are quite similar. However, the central values of q are distinct. With LHCD, q tends to increase to very high values, such as $q_0 \approx 30$–50 whereas in the case of ECCD, q_0 remains between 10 and 20. This difference comes mainly from the amount of driven off-axis current; LHCD driven current is of the order of 500–900 kA whereas ECCD current is only 70–160 kA. The large off-axis current can transiently drive the total current density in the core to zero, as has been recently observed in JET. This is investigated in more detail in Section 3.2.2 and Publication 4. Category 2 consists of off-axis NBI

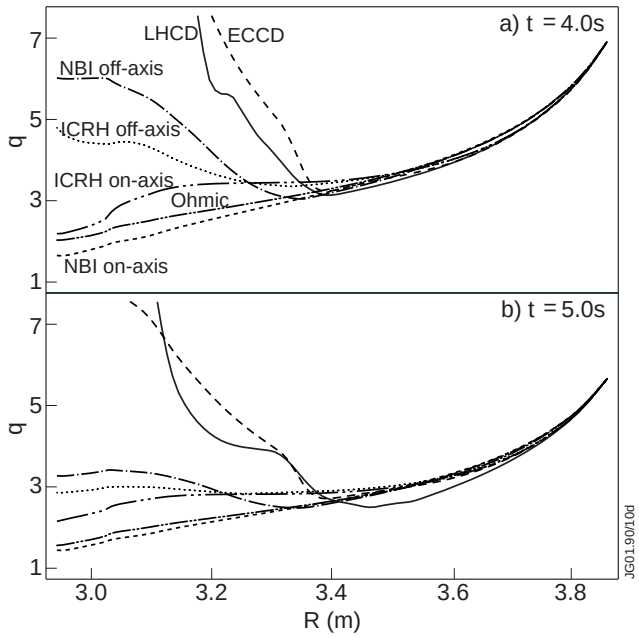

Figure 3.3: Simulated q-profiles produced with different preheating methods at $t = 4.0$ s (a) and $t = 5.0$ s (b). Category 1: LHCD (solid curve) and ECCD (dashed curve); category 2: off-axis NBI (dash-dotted curve) and off-axis ICRH (dotted curve); category 3: on-axis NBI (short dashed curve), on-axis ICRH (long double dot-dashed curve) and ohmic (short double dot-dashed curve).

and off-axis ICRH heating which create weakly reversed q-profiles with $q_{\min}$ located inside $R = 3.4$ m. On-axis NBI, on-axis ICRH and ohmic preheating belong to category 3 as they can only create monotonic q-profiles. Experimental results on LHCD, ICRH and Ohmic preheating on JET, presented in Publication 3 and Ref. [118], have verified the aforementioned predictive modelling results.

One of the main conclusions in this study is that the external current driven by LHCD and ECCD, not the decreased current diffusion by the direct electron heating, is the crucial factor in producing deeply reversed target q-profiles in the preheating phase. Also, the NBI driven current turned out to be very important in the off-axis NBI preheating scheme. Other important factors affecting the q-profile evolution in the preheating phase are the width of the power deposition profile and the start time of the preheating with respect to plasma initialisation. A narrow off-axis power deposition profile is able to slow down the ohmic current diffusing from the plasma periphery to the centre much more efficiently than a wide one. Moreover, the earlier the preheating is started, the more the current diffusion is slowed down. Since ICRF preheating has wider power deposition profiles than ECRH and it also has an additional slowing down time of the fast ions colliding with the electrons (≈ 0.5 s in JET) that is missing in the ECRH scheme, it is

understandable that ECRH preheating (even without any ECCD current) turned out to be a more efficient tool to modify the q-profile evolution in the preheating phase than ICRH.

How well the desired target q-profile can be sustained later in the main heating phase depends on the applied heating and current drive methods and the power levels. Bootstrap current and its alignment with the desired current density profile becomes an important issue. The current density evolution in the main heating phase has been analysed in Section 3.2.3 and Publication 5. It should be noted that the experimental results on the q-profile evolution in the preheating phase from other tokamaks may differ from the present results. These differences originate from the different machine sizes and heating systems with different power densities.

3.2.2 Core Current Hole with LHCD Preheating in JET

An observation of zero current density within measurement errors in the core ($r/a \leq 0.2$) of JET 'Advanced Tokamak Scenario' plasmas with LHCD preheating is reported in Publication 4. This is the first time ever in any tokamak when a so-called core current hole has been observed. Theoretically it has been predicted earlier that a region of zero or even negative $j(R)$ in the core can exist [119, 120]. According to the theory, the total magnetic flux, and therefore the total current, in the core of a highly conductive plasma cannot be rapidly modified due to the slow radial diffusion of the parallel electric field. It can be seen from the following expression, obtained by combining in a cylindrical geometry the radial derivative of the Faraday's law with the time derivative of the Ampère's law and then eliminating the axial electric field using the Ohm's law:

$$\frac{\partial j_{\mathrm{tot}}}{\partial t} = \mu_0^{-1} \left(\frac{\partial^2}{\partial r^2} + \frac{1}{r}\frac{\partial}{\partial r} \right) \eta_{||}(j_{\mathrm{tot}} - j_{\mathrm{ext}}). \tag{3.1}$$

Here, j_{tot} is the total parallel current density, j_{ext} is the externally driven (non-inductive) parallel current density, and $\eta_{||}$ is the parallel resistivity. Initially the external current drive is switched off ($j_{\mathrm{ext}} = 0$). When the external off-axis current drive turns on, regions of positive radial curvature ($\frac{\partial^2}{\partial r^2}\left[\eta_{||}(j_{\mathrm{tot}} - j_{\mathrm{ext}})\right]$) on either side of the peak in j_{ext} transiently decrease j_{tot}. With sufficient external current, this effect can locally drive the current density to zero or even negative. This situation can persist for many seconds in hot JET plasmas due to the long current diffusion time.

The experimentally observed core current hole can be seen in a simulation of the evolution of the current density performed with JETTO. Measured values of the densities, temperatures, Z_{eff}, plasma current and magnetic field are used. The simulation is started at $t = 1.0$ s and the initial q-profile is taken from the EFIT equilibrium.

Figure 3.4 shows the simulated current density profiles at two times, during the LHCD prelude at $t = 3.0$ s and immediately afterwards that at $t = 4.0$ s. The

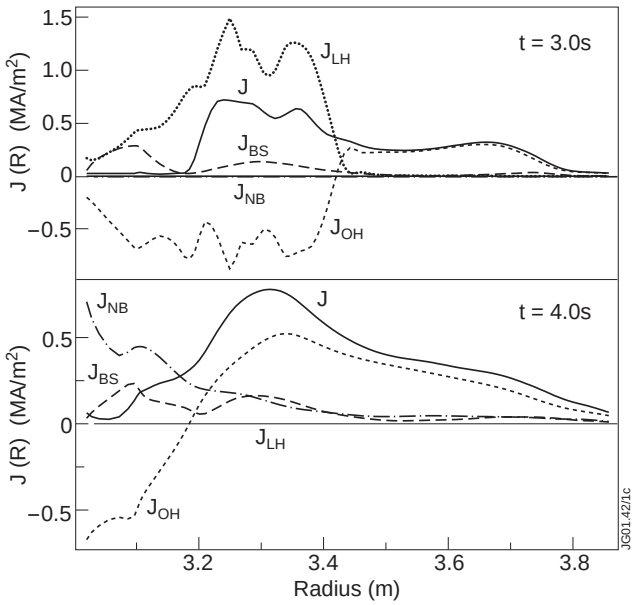

Figure 3.4: JETTO *simulation of $j(R)$ during the LHCD preheating phase ($J_{\rm NB} = 0$) at $t = 3.0$ s and immediately after ($J_{\rm LH} = 0$) at $t = 4.0$ s. The contributions to the total current due to LHCD ($J_{\rm LH}$), Ohmic current ($J_{\rm OH}$), bootstrap current ($J_{\rm BS}$) and beam-driven current ($J_{\rm NB}$) are shown. The region of the core current hole is clearly visible at $t = 3.0$ s.*

contributions to the total current due to LHCD, Ohmic current, bootstrap current, and beam-driven current are shown. The region of zero current density in the core region ($r/a \leq 0.2$) at $t = 3.0$ s created in response to the strong off-axis LHCD is illustrated in Figure 3.4. At $t = 4.0$ s the region of zero current begins to fill in after the LHCD turns off, leaving a small region of zero current density similar to that deduced from the Motional-Stark Effect (MSE) measurements. Shrinking of the region of zero current is significantly enhanced by the on-axis current driven by the neutral beams present at $t = 4.0$ s but not at $t = 3.0$ s. The modelling is qualitatively consistent with the MSE measurements.

The resistivity, LHCD power deposition and bootstrap current profile calculations are not valid in the regime where the toroidal current vanishes, while the profiles away from the zero current region will still be valid. In the JETTO simulations, this situation is avoided by enforcing $q < 60$. However, the fact that this condition of the zero current, i.e. $q \to \infty$, in the core is attained in the JETTO simulation is a confirmation of the mechanism suggested as responsible for the zero axis current. In addition, the use of the $q < 60$ is justified by the experimental measurements which indicate that the current in the core is not negative, but seems to be clamped at zero. This observation suggests that a separate physical mechanism acts to prevent a negative core current density to exist. It is possible that the sawtoothlike MHD

modes present during the LHCD prelude could redistribute the current from the periphery to the zero $j(R)$ region, thus preventing formation of a negative $j(R)$ region [121], but this has not yet been experimentally verified.

3.2.3 Improved Fusion Performance with Current Profile Control

The performance of the 'Advanced Tokamak Scenarios' is investigated and optimised with JETTO transport code modelling calculations, using LHCD for current profile control. As found in Publication 3, LHCD can create hollow current density profiles and a wide region of negative magnetic shear. Therefore, as the empirical studies in Publication 1 indicated, wider ITBs with a steep pressure gradient producing large amount of bootstrap current can be achieved. However, there is only a very limited number of high performance 'Advanced Tokamak Scenario' experiments with current profile control by LHCD performed on JET. The main reason for this is due to the problems in the coupling of the LHCD with the H-mode plasma edge. It is therefore crucial to investigate how LHCD, applied to high performance discharges, affects the sustainability of the ITB and plasma performance on JET.

The starting point for the modelling calculations of the high performance discharges is the pulse No. 40542. In the experiment, the high performance phase lasted from $t = 5.0$ s until $t = 7.5$ s, but the modelling calculation is extended by 5.5 s until $t = 13.0$ s. The reason for choosing this pulse is that it has suitable steady-state like features and benign properties against MHD instabilities. The initial and boundary conditions for T_i, T_e, n_e and plasma current are taken from the experiment. The plasma current is as for the actual discharge No. 40542 until $t = 7.5$ s after which it is ramped-up up to 3.9 MA at the same speed. The magnetic field is taken from the experiment ($B = 3.4$ T) as well as Z_eff. The heating power and the deposition profiles of NBI and ICRH are kept fixed since the last experimental power deposition profiles calculated by TRANSP [122]. The LH power deposition profiles, which are the key issue in the modelling calculations, are calculated self-consistently by JETTO/FRTC. This new coupled code combination is validated in Publication 5. The transport model is the same as shown in Eqs. (2.14)–(2.20) with the exception of some differences in the argument of the step function in the ITB formation condition (see Publication 5).

The time evolution of the fusion power is shown in Figure 3.5 (a) (upper half). As can be seen, fusion power in the range 20–30 MW is predicted for $I_\mathrm{p} = 3.9$ MA, $B_\mathrm{t} = 3.4$ T discharges. There are three types of uncertainties in the modelling; uncertainties coming from the experimental data, like the initial q-profile and the boundary values for T_i and T_e, uncertainties coming from the LHCD module, such as the amount of LH driven current and those ones coming from the transport model, like the empirical fitting parameter used in the ITB formation threshold condition. The shaded area illustrates the modelling uncertainties; the upper curve is a prediction with the present transport model using the experimental data as it is

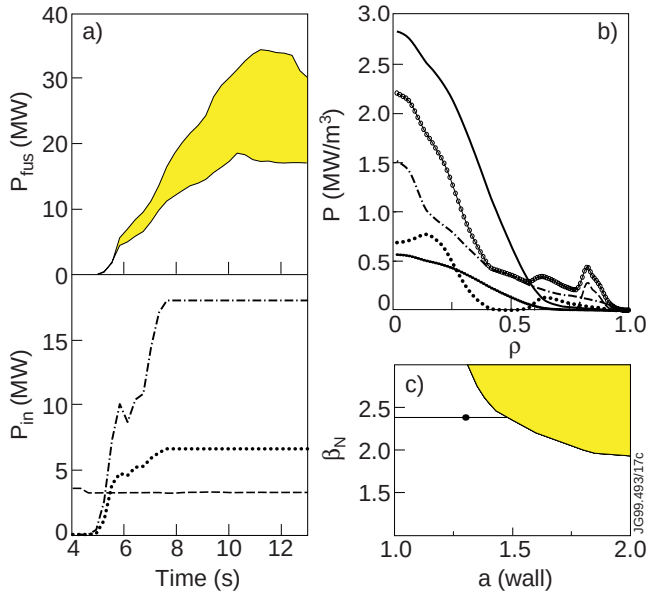

Figure 3.5: (a) Time evolution of the fusion power with modelling uncertainties predicted by JETTO/FRTC *and the input heating powers (NB=dash-dotted, RF=dotted, LH=dashed). (b) The radial profiles of the input heating powers (NB=dash-dotted, RF=dotted, LH=dashed, NB+RF+LH=solid curve with circles) and produced fusion (solid curve) and alpha heating powers (densely dotted) at $t = 13.0$ s. (c) MHD stability analysis of the scenario with the largest fusion power at $t = 13.0$ s. The shaded area is unstable against the $n = 1$ kink instability as being the limiting factor.*

while the lower curve represents a conservative prediction assuming lower recycling coefficient for the neutrals penetrating back to the plasma at the edge and lower edge temperatures. The case with the larger fusion power is stable against MHD instabilities with a beta value $\beta_N \approx 2.4$, as illustrated in Figure 3.5(c). The most limiting MHD instability is the pressure driven global $n = 1$ kink instability which is a typical limiting factor for the high performance 'Advanced Tokamak Scenario' discharges on JET [123]. Worth mentioning is that the MHD stability analysis does not consider neo-classical tearing modes nor $q = 2$ snakes which often limit the high performance in JET. Therefore, the fusion power may be overestimated. The input heating powers of $P_{NB} = 18$ MW, $P_{RF} = 6.5$ MW (composed of 2/3 on-axis and 1/3 off-axis deposition) and $P_{LH} = 3.5$ MW are illustrated in Figure 3.5(a) (bottom) and the power deposition profiles in (b), respectively.

The quasi-stationary regimes for electron and ion temperatures as well as for densities, pressure and the location of the ITB are reached at $t \approx 10$ s. The current diffusion time is around 40–50 s. The magnetic shear is negative inside about 60–70 % of the plasma radius. The safety factor at the edge (q_{95}) is between 3 and 4

and settles during the steady state phase down to 3.1. Worth noticing is also the large contribution (≈ 50 %) from the bootstrap current which is produced in the large pressure gradient region, i.e. in the same region where the footpoint of the ITB is located, thus giving rise to larger current and smaller magnetic shear in that region. An interesting question remains whether this scenario could be extended to true steady-state, i.e. being independent of the current diffusion time. It would require enough off-axis current produced by the bootstrap current together with LHCD to compensate the slow current diffusion.

The same two simulations as shown in Figure 3.5 are also performed without LHCD. In each run, the ITB is formed slightly later and its width stays about 10 cm narrower until $t = 7.0$ s than in the simulation with LHCD. After $t = 7.0$ s the ITB starts to shrink and finally at $t \approx 8$ s, the width of the ITB settles down to $\rho \approx 0.4$. The fusion power is only about 50–60 % of the fusion power with LHCD and the average ion temperature about 80 %. The reason for the degraded fusion performance and confinement is that the q-profile remains monotonic (positive magnetic shear) throughout the discharge, thus inhibiting the ITB to lie on a larger radius [124].

Different current ramp-up schemes are also analysed for 'Advanced Tokamak Scenario' plasmas with JETTO. In the core region the current density profiles are not affected, but at $\rho > 0.4$ they are strongly modified. ITBs are wider with a larger current and with a faster current ramp-up speed. In conclusion, shrinking of the ITBs seems to be caused by higher edge shear, i.e. higher q_{a} (smaller I_{p}). Consequently, the best fusion performance for the 'Advanced Tokamak Scenario' plasmas is expected to be obtained with the highest current and the fastest stable current ramp-up speed.

Chapter 4

Summary and Conclusions

This thesis is about transport modelling of 'Advanced Tokamak Scenarios' in the Joint European Torus (JET). Answers to and explanations for the following questions have been sought: what are the mechanisms that govern the formation and dynamics of the ITBs in JET and how can the current density profile be modified and further, how does the current density profile affect ITBs and plasma performance? In order to reliably predict the performance perspectives in future 'Advanced Tokamak Scenarios' in JET and ITER, it is crucial to know and understand the answers to the aforementioned questions.

On the basis of the results from the transport analyses carried out during the course of this thesis, two possible scenarios for the ITB formation and for the time evolution of the ITB in JET can be illustrated. The first one (scenario 1) is based on the empirical studies of the $\omega_{\mathrm{E\times B}}$ flow shear and magnetic shear, together with predictive modelling with the Bohm/GyroBohm transport model, whereas the second scenario (scenario 2) is based on the results from the Weiland fluid theory. In scenario 1, the onset of the ITB occurs provided that the threshold condition $s \leq 1.47\omega_{\mathrm{E\times B}}/\gamma_{\mathrm{ITG}} + 0.14$ given in Eq. (2.8) is fulfilled. Triggering of the ITB is probably initiated around a magnetic island at an integer q surface when the condition in Eq. (2.8) is approached, and the $\omega_{\mathrm{E\times B}}$ shearing rate is locally enhanced because of the island. In the ITB formation, according to the found empirical ITB threshold condition, the following interaction between the $\omega_{\mathrm{E\times B}}$ shearing rate and s could occur: the $\omega_{\mathrm{E\times B}}$ flow shear must be large enough to tear apart the turbulent eddies, thus decreasing the growth rate of the long wave length ITG turbulence (γ_{ITG}). At the same time the small (or negative) magnetic shear s helps to disconnect the turbulent vortices (e.g. ballooning modes) initially linked together by toroidicity and enables the plasma to enter the second stable ballooning stability region. The found empirical threshold condition for the ITB formation provides the first clear indication of the strong correlation between s and $\omega_{\mathrm{E\times B}}$ at the ITB transition in JET. The modelling results from the extensive predictive transport analyses with the found empirical ITB threshold condition in Eq. (2.8)

support the strong interplay between $\omega_{\mathrm{E}\times\mathrm{B}}$ and s in governing the dynamics of the ITB in JET.

The ITB formation scenario 2 is based mainly on the density gradient stabilisation. The threshold of the critical ion temperature gradient length $L_{\mathrm{T_i}}^{\mathrm{crit}}$ to have the ITG turbulence unstable depends on the density gradient. Therefore, having a larger density gradient allows one also to have a larger temperature gradient while preventing the ITG micro-turbulence from becoming unstable at the same time. Consequently, a large density gradient can act as an ITB formation mechanism. Again, the onset of the ITB may be initiated at an integer q surface around which the density gradient locally increases. Furthermore, a small or negative magnetic shear facilitates the ITB formation, probably in a similar way as in the ITB formation scenario 1. In addition, after having formed an ITB, the significantly enhanced $\omega_{\mathrm{E}\times\mathrm{B}}$ flow shear may help to stabilise TEM which may be otherwise destabilised by the density gradient. The modelling results from the predictive transport simulations with the Weiland model emphasise strongly the importance of the density gradient over the $\omega_{\mathrm{E}\times\mathrm{B}}$ shearing rate in governing the dynamics of the ITB. In addition, the good confinement in the so-called Pellet Enhanced Performance (PEP) mode observed in JET 10 years ago was also explained to be due to the favourable effects provided by the large density gradient [107].

There are two major problems in analysing the ITB formation mechanisms — the interplay and the coupling of the different mechanisms with each other. Due to the interplay, it may be difficult to identify which mechanism is the dominant one, as in the case when one employs the empirical ITB threshold condition in Eq. (2.8). The coupling problem can be seen when one increases for example n_{e} by NBI fuelling or pellets, both the density gradient and the Shafranov shift increase and in addition, the $\omega_{\mathrm{E}\times\mathrm{B}}$ shearing rate may increase or decrease. Therefore, due to the coupling of the different ITB formation mechanisms, diagnosing the principal mechanism is tricky. Consequently, the causality, i.e. the classical "which was first, hen or egg" problem, is difficult to resolve. In the ITB formation scenario 1, the $\omega_{\mathrm{E}\times\mathrm{B}}$ shearing rate seems to be the cause of the ITB, together with s whereas in scenario 2, the density gradient seems to be the cause while the $\omega_{\mathrm{E}\times\mathrm{B}}$ shearing rate is rather the effect of the ITB than the cause.

At first glance, it is quite astonishing that the two aforementioned scenarios 1 and 2, which are based on completely different physics mechanisms, seem both to be able to explain the ITB formation and time evolution in JET. One of the most plausible reasons for this coincidence is that in JET, the NBI is the main source for both the $\omega_{\mathrm{E}\times\mathrm{B}}$ flow shear through the toroidal momentum injection and for the increase of the density gradient through the core particle fuelling. As a consequence, when one increases the NBI power, one increases the toroidal momentum and particle fuelling simultaneously. Due to the relatively inflexible NBI system in JET, keeping the same NBI power and thus the same fuelling, the amount of the toroidal momentum is difficult to change [125]. By replacing a part of the NBI power with the ICRH power, one encounters the same problem; both the fuelling and the toroidal momentum injection are decreased in a similar way. One way to resolve the problem would be to increase the density gradient in the

core with pellets as in the PEP mode [107] and see whether an ITB appears in this 'Advanced Tokamak Scenario'. Launching a significant amount of pellets in the core, the density gradient should rise while the $\omega_{\mathrm{E}\times\mathrm{B}}$ flow shear should not change significantly, only the pressure gradient term in Eq. (2.6) may change a little, but it should not affect the $\omega_{\mathrm{E}\times\mathrm{B}}$ shearing rate very much.

One common thing that is not controversial among the ITB formation mechanisms is that the small or negative magnetic shear facilitates the ITB formation. Still, it is not clear in which way the magnetic shear affects the ITB formation. The ITB formation scenario 1 would suggest that zero or negative s is enough to form an ITB. However, the effect of the magnetic shear could also be only that the smaller is the magnetic shear, the smaller $\omega_{\mathrm{E}\times\mathrm{B}}$ shearing rate or the smaller density gradient is needed to stabilise micro-turbulence and to form an ITB. In addition, it is still not clear whether the value $s = 0$ has a special role in the ITB physics or whether the condition reads rather like $s \lessapprox 0$.

The second main topic in this thesis considered the modelling of the current density profile and its impacts on the ITB formation and plasma performance. On the basis of the transport simulations in the preheating phase, the heating and current drive methods could be divided into three categories in terms of the produced q-profiles. LHCD and ECCD formed category 1 since they were the only methods which created deeply reversed q-profiles in JET. Accordingly, in order to have the maximum flexibility for creating the desired q-profile in the preheating phase, either the LHCD or the ECCD system is to be installed in future tokamaks. Category 2 consisted of off-axis NBI and off-axis ICRH preheating which produced weakly reversed q-profiles with q_{min} located inside $R = 3.4$ m. On-axis NBI and on-axis ICRH and ohmic preheating belonged to category 3 as they created only monotonic q-profiles. Experimental results on LHCD, ICRH and Ohmic preheating on JET verified the predictive modelling results (Publication 3).

It has been argued for a long time, for example in the case of LHCD, whether it is the effect of the direct electron heating that decelerates the ohmic current diffusion or whether it is the external off-axis current driven by LHCD which is the main contributor in modifying the current density profile in JET. In this thesis, the external current driven by LHCD, ECCD or NBI was found to be the most crucial factor in giving the best flexibility to modify q-profiles in the preheating phase. Other important factors affecting the q-profile evolution in the preheating phase were found to be the width of the power deposition profile and the start time of the preheating with respect to plasma initialisation. A narrow off-axis power deposition profile was able to slow down the ohmic current diffusing from the plasma periphery to the centre much more efficiently than a wide one. Moreover, the earlier was the preheating started, the more was the ohmic current diffusion slowed down.

As a fascinating special case of LHCD preheating, the so-called core current hole was introduced in this thesis. The existence of the core current hole can be explained by combining the Faraday's, Ampere's and Ohm's laws. Then, a sufficient amount of off-axis current can locally and transiently drive the current density to zero in the core. In JET, this situation can persist for many seconds due to the

long current diffusion time. Predictive JETTO simulations confirmed the presented physical picture as the condition $q \to \infty$ ($j \to 0$) in the core was attained in the JETTO calculations. Even if it seems possible and even probable that a plasma with the core current hole is not an optimum way to operate the 'Advanced Tokamak Scenario', it may be very enlightening from physics' point of view. This new plasma regime with a region of the core current hole found in Publication 4 poses several new challenges and requirements on transport modelling. The new regime also suggests interesting experiments with promising perspectives of finding new physics. Firstly, it enforces the neo-classical theory used in transport models to be modified since the present neo-classical transport theory is not valid when B_θ is close to zero. Secondly, it will allow studies on the dependence of the $\omega_{\mathrm{E}\times\mathrm{B}}$ on B_θ and a possible further impact on the ITB formation because B_θ is almost zero in the region of the current hole and outside the region has a large gradient. Thirdly, the calculation of the equilibrium must be updated. For example EFIT and ESCO reconstruct the equilibrium as a function of the poloidal magnetic flux whose definition will not be single-valued with the core current hole. Therefore, the equilibrium reconstruction does not converge towards an unique equilibrium and the flux surfaces remain undefined.

It is not yet known exactly what the optimal q-profile in the 'Advanced Tokamak Scenarios' will be. One of the most important criteria is that it should facilitate the formation of the optimal ITB profile, which was sketched in Figure 2.3, and prevent the non-optimal ITB profile from arising. As a consequence, the optimal q-profile should assist the ITB to form as wide as possible in r/a (broad T_i, T_e and n_e profiles) and with moderate gradients. The optimal q-profile should also provide the largest sustainable improvement in the fusion performance and a good confinement while at the same time it should be MHD stable against large-scale MHD instabilities.

Obviously in the optimal 'Advanced Tokamak Scenario', the optimal ITB profile should be somehow combined with the optimal q-profile. However, achieving the optimal 'Advanced Tokamak Scenario' is not trivial for at least two basic reasons; firstly, it is not yet known precisely what the optimal ITB and q-profiles are and secondly, reaching experimentally the optimal ITB and q-profiles is a difficult task. As found in Publication 5, application of LHCD during the high performance phase helps in achieving the optimal ITB and q-profiles. With LHCD, s is smaller and an ITB can more easily expand. A larger ITB radius leads then to a larger fraction of the bootstrap current, which further decreases the magnetic shear. At the same time the plasma performance is enhanced. In addition, a larger ITB radius is more benign against MHD instabilities. Although LHCD and NB current drive may be of importance in optimising the q-profile, the importance of the bootstrap current and its alignment with the optimal q-profile is probably even greater, in particular in future large tokamaks like in ITER.

A large ITB radius implies also a moderate or steep density gradient at a large radius. In the light of the modelling results in Publication 2, obtaining moderate or steep density gradients may be crucial if it can stabilise the ITG since the ITG is the worst possible branch of turbulence in terms of the amount of transport it

drives. Having stabilised the ITG and possibly the ETG with the density gradient, it may be then easier to stabilise the TEM, which is not stabilised by the density gradient, through the $\omega_{\mathrm{E}\times\mathrm{B}}$ flow shear, the Shafranov shift or the negative magnetic shear.

In the integrated modelling of the ITB dynamics and current density profile in the 'Advanced Tokamak Scenarios', it should be noted, however, that certain important aspects have not been considered in this thesis. Firstly, as it has been indicated in Publication 2, a moderate or steep density gradient may stabilise micro-turbulence, like the ITG and enable the optimal ITB profile to be born. However, according to neo-classical theory, the impurity accumulation in the core due to the density gradient is a very serious problem. The impurity accumulation in the 'Advanced Tokamak Scenarios' with a moderate and steep density gradient has been also verified in the experiments in JET [126]. This may limit significantly the range of the feasible density gradients in the 'Advanced Tokamak Scenarios'. Secondly, as it has been demonstrated in Publications 3 and 4, LHCD is a very useful tool in modifying the current density profile. However, there are serious problems in the coupling of the LH waves from the grill to the plasma in the H-mode discharges with ELMs. Thus, the LH power and current may be overestimated in the modelling calculations. Thirdly, large scale MHD events, such as NTMs and ELMs, are not taken into account in the modelling. These may change the behaviour of the ITBs and limit significantly the feasible pressure, temperature, density and current density profiles in the 'Advanced Tokamak Scenarios'.

Bibliography

[1] Ongena J. and van Oost G., "Energy for Future Centuries", Transactions of Fusion Technology **37** (2000) 3.

[2] Kadomtsev B.B., *Tokamak plasma, a complex physical system*, Institute of Physics Publishing, Bristol, 1992.

[3] Wesson J., *Tokamaks*, Oxford Science Publications, Oxford, 1997.

[4] Golowin I.N. and Schafranov W.D., *Die Anfänge der Kontrollierten Kernfusion (in Andrej D. Sacharow, Leben und Werk einers Physikers)*, Spektrum Akad. Verlag, Heidelberg, 1991, p. 45.

[5] Tamm I.E. and Sakharov A.D., *Plasma Physics and the Problem of Controlled Thermonuclear Reactions*, edited by M.A. Leontovich, Pergamon Press, London, 1961, Vol. 1.

[6] Artsimovich L.A. et al., "Experiments in tokamak devices", Plasma Physics and Controlled Nuclear Fusion Research (Proc. Int. Conf., Novosibirsk, 1968), IAEA, Vienna, **1** (1969) 157.

[7] Wagner F. et al., "Regime of improved confinement and high beta in neutral-beam heated divertor discharges of the ASDEX tokamak", Phys. Rev. Lett. **49** (1982) 1408.

[8] Keilhacker M. et al., "High fusion performance from deuterium-tritium plasmas in JET", Nucl. Fusion **39** (1999) 209.

[9] de Baar M.R., *Electron Transport Barriers in Tokamak Plasmas*, PhD Thesis, FOM Institute, The Netherlands, (1999).

[10] Fisch N.J., "Theory of current drive in plasmas", Reviews of Modern Physics **59** (1987) 175.

[11] Cairns R.A., *Radiofrequency Heating of Plasmas*, Institute of Physics Publishing, Bristol, 1991.

[12] Hinton F.L. and Hazeltine R.D., "Theory of plasma transport in toroidal confinement systems", Rev. Mod. Phys. **48** (1976) 239.

[13] Hirshman S.P. and Sigmar P.D., "Neoclassical transport of impurities in tokamak plasmas", Nucl. Fusion **21** (1981) 1079.

[14] Taguchi M., "A method for calculating neoclassical transport coefficients with momentum conserving collision operator", Phys. Fluids B **4** (1992) 3638.

[15] Koide Y. et al., "Internal Transport Barrier on $q = 3$ Surface and Poloidal Plasma Spin Up in JT-60U High-β_p Discharges", Phys. Rev. Lett **72** (1994) 3662.

[16] Levinton F.M. et al., "Improved Confinement with Reversed Magnetic Shear in TFTR", Phys. Rev. Lett. **75** (1995) 4417.

[17] Strait E.J. et al., "Enhanced Confinement and Stability in DIII-D Discharges with Reversed Magnetic Shear", Phys. Rev. Lett. **75** (1995) 4421.

[18] The JET Team (presented by C. Gormezano), "Optimisation of JET Plasmas with Current Profile Control", Proc. 16th Int. Fusion Energy Conf. Montreal, Canada, 7–11 October 1996, **1** IAEA, Vienna (1997) 487.

[19] Söldner F.X. et al., "Shear optimization experiments with current profile control on JET", Plasma Phys. Control. Fusion **39** (1997) B353.

[20] Parail V.V. et al., "Predictive Modelling of JET Optimised Shear Discharges", Nucl. Fusion **39** (1999) 1743.

[21] Baranov Yu.F. et al.,"Current profile, MHD activity and transport properties of optimised shear plasmas in JET", Nucl. Fusion **39** (1999) 1463.

[22] Shirai H. et al., "Recent experimental and analytic progress in the Japan Atomic Energy Research Institute Tokamak-60 Upgrade with W-shaped divertor configuration", Phys. Plasmas **5** (1998) 1712.

[23] Greenfield C.M. et al., "Behaviour of electron and ion transport in discharges with internal transport barrier in the DIII-D tokamak", Nucl. Fusion **39** (1999) 1723.

[24] Gruber O. et al., "Stationary H-Mode Discharges with Internal Transport Barrier on ASDEX Upgrade", Phys. Rev. Lett. **83** (1999) 1787.

[25] Erba M. et al., "Validation of a New Mixed Bohm/gyro-Bohm Transport Model on Discharges of the ITER Data-Base", JET Report JET-R(96)07 (1996).

[26] Erba M. et al., "Development of a non-local model for tokamak heat transport in L-mode, H-mode and transient regimes", Plasma Phys. Control. Fusion **39** (1997) 261.

[27] Genacchi G. and Taroni A., "JETTO: A free boundary plasma transport code (basic version)", Rapporto ENEA RT/TIB 1988(5).

[28] Jarmen A., Andersson P. and Weiland J., "Fully toroidal ion temperature gradient driven drift modes", Nucl. Fusion **27** (1987) 941.

[29] Nordman H., Weiland J. and Jarmen A., "Simulation of toroidal drift mode turbulence driven by temperature gradients and electron trapping", Nucl. Fusion **30** (1990) 983.

[30] Weiland J. and Hirose A., "Electromagnetic and kinetic effects on the ion temperature gradient mode", Nucl. Fusion **32** (1992) 151.

[31] Strand P., Nordman H., Weiland J. and Christiansen J., "Predictive transport simulations of JET L and H mode gyro-radius scaling experiments", Nucl. Fusion **38** (1998) 545.

[32] Esterkin A.R. and Piliya A.D., "Fast ray tracing code for LHCD simulations", Nucl. Fusion **36** (1996) 1501.

[33] Nowak S., Lazzaro E. and Ramponi G., "Self-diffraction effect of electron cyclotron Gaussian beams on noninductively driven current in the International Thermonuclear Experimental Reactor tokamak", Phys. Plasmas **3** (1996) 4140.

[34] Challis C.D. et al., "Non-inductively driven currents in JET", Nucl. Fusion **29** (1989) 563.

[35] ITER Physics Basis Editors, et al., "Plasma confinement and transport", Nucl. Fusion **39** (1999) 2175.

[36] JET TEAM (presented by D. Stork), "The new experimental phase of JET and prospects for future operation", in Plasma Physics and Controlled Nuclear Fusion Research 1994 (Proc. 15th Int. Conf. Seville, 1994), **1**, IAEA, Vienna (1995) 51.

[37] Wade M. et al., "Helium Exhaust Studies in H-Mode Discharges in the DIII-D Tokamak Using an Argon-Frosted Divertor Cryopump", Phys. Rev. Lett. **74** (1995) 2702.

[38] Koide Y. et al., "Study of internal transport barriers by comparison of reversed shear and high-$\beta_{\rm p}$ discharges in JT-60U", Plasma Phys. Control. Fusion **40** (1998) 641.

[39] Lazarus E.A. et al., "Higher Fusion Power Gain with Current and Pressure Profile Control in Strongly Shaped DIII-D Tokamak Plasmas ", Phys. Rev. Lett. **77** (1996) 2714.

[40] Ishida S. and JT-60U Team, "JT-60U high performance regimes", Nucl Fusion **39** (1999) 1211.

[41] Parail V.V., "Energy and particle transport in plasmas with transport barriers", to be published in Plasma Phys. Control. Fusion (2002).

[42] Horton W., Hong B.-G. and Tang W.M., "Toroidal electron temperature gradient driven drift modes", Phys. Fluids, **31** (1988) 2971.

[43] Weiland J., *Collective Modes in Inhomogenous Plasma*, Institute of Physics Publishing, Bristol, 2000.

[44] Garbet X. et al. "Turbulence in fusion plasmas: key issues and impact on transport modelling", Proc. 28th European Physical Society Conf. on Controlled Fusion and Plasma Physics, Madeira, Portugal, 18-22 June, 2001 A251.

[45] Hasselberg G. and Rogister A., "Drift wave transport and origin of the disruption phenomenon — a theoretical model", Nucl. Fusion **23** (1983) 1351.

[46] Waltz R.E., Dominguez R.R. and Perkins F.W., "Drift wave model tokamak ignition projections with a zero-dimensional transport code", Nucl. Fusion **29** (1989) 351.

[47] Rechester A.B. and Rosenbluth M.N., "Electron Heat Transport in a Tokamak with Destroyed Magnetic Surfaces", Phys. Rev. Lett. **40** (1978) 38.

[48] Kadomtsev B.B. and Pogutse O.P., "Turbulence in Toroidal Systems", Reviews of Plasma Physics (ed. M.A. Leontovich) Consultants Bureau, New York, **5** (1970) 249.

[49] Beer M.A. et al., "Gyrofluid simulations of turbulence suppression in reversed-shear experiments on the Tokamak Fusion Test Reactor", Phys. Plasmas **4** (1997) 1792.

[50] Doyle E.J. et al., "Progress towards increased understanding and control of internal transport barriers (ITBs) on DIII-D", Proc. 18th Int. Fusion Energy Conf. Sorrento, Italy, 4–10 October 2000, paper IAEA-CN-77/EX6/2.

[51] Itoh K. et al., "L-mode confinement model based on transport-MHD theory in tokamaks", Plasma Phys. Control. Fusion **35** (1993) 543.

[52] Guzdar P.N., Drake J.F., McCarthy D. and Hassam A.B., "Three-dimensional fluid simulations of the nonlinear drift-resistive ballooning modes in tokamak edge plasmas", Phys. Fluids B **5** (1993) 3712.

[53] Connor J.W. and Chen L., "Resistive ballooning modes in an axisymmetric toroidal plasma with long mean free path", Phys. Fluids **28** (1985) 2201.

[54] Stober J. et al., "Effects of triangularity on confinement, density limit and profile stiffness of H-modes on ASDEX upgrade", Plasma Phys. Control. Fusion **42** (2000) A211.

[55] Horton L.D. et al., "Performance near operational boundaries", Plasma Phys. Control. Fusion **41** (1999) B329.

[56] Mantica P. et al. "Non-local plasma response induced by peripheral perturbations in the RTP tokamak", Proc. 24th European Physical Society Conf. on Controlled Fusion and Plasma Physics, Berchtesgaden, Germany, 9–13 June 1997, **1V** (1997) 1853.

[57] Hawryluk R.J. et al., "Confinement and Heating of a Deuterium-Tritium Plasma", Phys. Rev. Lett. **72** (1994) 3530.

[58] Greenwald M. et al., "A new look at density limits in tokamaks", Nucl. Fusion **28** (1988) 2199.

[59] Saibene G. et al. "The Effect of Plasma Shape on Density and Confinement of ELMy H-mode in JET", Proc. 28th European Physical Society Conf. on Controlled Fusion and Plasma Physics, Madeira, Portugal, 18-22 June, 2001 933.

[60] Efthimion P.C. et al., "Observation of Temperature-Dependent Transport in the TFTR Tokamak", Phys. Rev. Lett. **66** (1991) 421.

[61] Greenwald M. et al., "Transport experiments in Alcator C-Mod", Phys. Plasmas **2** (1995) 2308.

[62] Zastrow K.-D. et al., "Transfer rates of toroidal angular momentum during neutral beam injection", Nucl. Fusion **38** (1998) 257.

[63] Kim Y.B., Diamond P.H. and Groebner R.J., "Neoclassical poloidal and toroidal rotation in tokamaks", Phys. Fluids B **3** (1991) 2050.

[64] Mattor N. and Diamond P.H., "Momentum and thermal transport in neutral-beam heated tokamaks", Phys. Fluids **31** (1988) 1180.

[65] De Esch H.P.L., Stork D. and Weisen H., "Toroidal plasma rotation in JET", Proc. 17th European Physical Society Conf. on Controlled Fusion and Plasma Physics, Amsterdam, The Netherlands, 25–29 June 1990, **14 B, part I** (1990) 90.

[66] Scott S.D., "Correlations of heat and momentum transport in the TFTR tokamak", Phys. Fluids B **2** (1990) 1300.

[67] Spitzer L. and Härm R., "Transport phenomena in a completely ionized gas", Physical Review **89** (1953) 1953.

[68] Challis C.D. et al., "Effect of q-profile modification by LHCD on internal transport barriers in JET", Plasma Phys. Control. Fusion **43** (2001) 861.

[69] Biglari H., Diamond P.H. and Terry P.W., "Influence of sheared poloidal rotation on edge turbulence", Phys. Fluids B **2** (1990) 1.

[70] Synakowski E.J., "Formation and structure of internal and edge transport barriers", Plasma Phys. Control. Fusion **40** (1998) 581.

[71] Burrell K.H. et al., "Effects of $E \times B$ velocity shear and magnetic shear in the formation of core transport barriers in the DIII-D tokamak", Plasma Phys. Control. Fusion **40** (1998) 1585.

[72] Doyle E.J. et al., "Observation of simultaneous internal transport barriers in all four transport channels and correlation with turbulence behaviour in NCS discharges on DIII-D", Plasma Phys. Control. Fusion **42** (2000) A237.

[73] Sips A.C.C. et al., "Operation at high performance in optimized shear plasmas in JET", Plasma Phys. Control. Fusion **40** (1998) 1171.

[74] Söldner F.X. et al., "Approach to steady state high performance in DD and DT plasmas with optimized shear in JET", Nucl. Fusion **39** (1999) 407.

[75] Budger T., *Plasma Physics and the Problem of Controlled Thermonuclear Reactions*, edited by M.A. Leontovich, Pergamon Press, New York, 1951, Vol. 1, p .78.

[76] Lehnert B., "Short-Circuit of Flute Disturbances at a Plasma Boundary", Phys. Fluids **9** (1966) 1367.

[77] Burrell K.H., "Effects of $E \times B$ velocity shear and magnetic shear on turbulence and transport in magnetic confinement devices", Phys. Plasmas **4** (1997) 1499.

[78] Staebler G.M., "Theory of internal and edge transport barriers", Plasma Phys. Control. Fusion **40** (1998) 569.

[79] Diamond P.H. et al., "Dynamics of Transition to Enhanced Confinement in Reversed Magnetic Shear Discharges", Phys. Rev. Lett. **78** (1997) 1472.

[80] Ernst D.R. et al., "Unifying Role of Radial Electric Field Shear in the Confinement Trends of TFTR Supershot Plasmas", Phys. Rev. Lett. **79** (1998) 2454.

[81] Shirai H. et al., "Role of radial electric field and plasma rotation in the time evolution of internal transport barrier in JT-60U", Plasma Phys. Control. Fusion **42** (2000) A109.

[82] Gruber O. et al., "Internal transport barrier discharges on ASDEX upgrade: progress towards steady state", Plasma Phys. Control. Fusion **42** (2000) A117.

[83] Staebler G.M., Waltz R.E. and Wiley J.C., "The role of rotation in tokamak internal transport barriers", Nucl. Fusion **37** (1997) 287.

[84] Synakowski E.J. et al, "Roles of Electric Field and Shafranov Shift in Sustaining High Confinement in Enhanced Reversed Shear Plasmas on the TFTR Tokamak", Phys. Rev. Lett. **78** (1997) 2972.

[85] Hahm T.S. and Burrell K.H., "Flow shear induced fluctuation suppression in finite aspect ratio shaped tokamak plasma", Phys. Plasmas **2** (1995) 1648.

[86] Waltz R.E., Kerbel G.D., Milowich J. and Hammet G.W., "Advances in the simulation of toroidal gyro-Landau fluid model turbulence", Phys. Plasmas **2** (1995) 2408.

[87] Crisanti F. et al., "Analysis of the $E \times B$ flow shearing rate in JET ITB discharges", Nucl. Fusion **41** (2001) 883.

[88] Turnbull A.D., Taylor T.S., Lin-Liu Y.R. and St. John H., "High Beta and Enhanced Confinement in a Second Stable Core VH-Mode Advanced Tokamak", Phys. Rev. Lett. **75** (1995) 718.

[89] Kessel C., Manickam J., Rewoldt G. and Tang W.M., "Improved Plasma Performance in Tokamaks with Negative Magnetic Shear", Phys. Rev. Lett. **72** (1994) 1212.

[90] Shaing K.C., Aydemir A.Y., Houlberg W.A. and Zarnstorff M.C., "Theory of Enhanced Reversed Shear Mode in Tokamaks", Phys. Rev. Lett. **80** (1998) 5353.

[91] Guo S.C. and Weiland J., "Analysis of η_{i} mode by reactive and dissipative descriptions and the effects of magnetic q and negative shear on the transport", Nucl. Fusion **37** (1997) 1095.

[92] Dorland W., Jenko F., Kotschenreuther M. and Rogers B.N., "Electron Temperature Gradient Turbulence", Phys. Rev. Lett. **85** (2000) 5579.

[93] Greenfield C.M. et al., "Understanding and control of transport in Advanced Tokamak regimes in DIII-D", Phys. Plasmas **7** (2000) 1959.

[94] Wolf R.C. et al., "Response of internal transport barriers to central heating and current drive on ASDEX Upgrade", Phys. Plasmas **7** (2000) 1839.

[95] Tala T.J.J. et al., "ITB Formation in Terms of $\omega_{\mathrm{E}\times\mathrm{B}}$ Flow Shear and Magnetic Shear s on JET", Proc. 27th European Physical Society Conf. on Controlled Fusion and Plasma Physics, Budapest, Hungary, 12-16 June, 2000 1493.

[96] Koide Y. and JT-60U Team, "Progress in confinement and stability with plasma shape and profile control for steady-state operation in the Japan Atomic Energy Research Institute Tokamak-60 Upgrade", Phys. Plasmas **4** (1997) 1623.

[97] Litaudon X. et al., "Stationary magnetic shear reversal experiments in Tore Supra", Plasma Phys. Control. Fusion **38** (1996) 1603.

[98] Joffrin E., Challis C.D., Hender T.C., Howell D.F. and Huysmans G.T.A., "MHD Internal Transport Barrier triggering in low positive shear scenario in JET", Nucl. Fusion **42** (2002) 235.

[99] Lopes Cardozo N.J. et al., "Electron thermal transport in RTP: filaments, barriers and bifurcations", Plasma Phys. Control. Fusion **39** (1997) B303.

[100] Fitzpatrick R., Hastie R.J., Martin T.J. and Roach C.M., "Stability of coupled tearing modes in tokamaks", Nucl. Fusion **33** (1993) 1533.

[101] Hogeweij G.M.D., Lopes Cardozo N.J., de Baar M.R. and Schilham A.M.R., "A model for electron transport barriers in tokamaks, tested against experimental data from RTP", Nucl. Fusion **38** (1998) 1881.

[102] Staebler G.M., "Density gradient bifurcation in tokamaks", Nucl. Fusion **39** (1999) 815.

[103] Lao L. et al., "Reconstruction of current profile parameters and plasma shapes in tokamaks", Nucl. Fusion **25** (1985) 1611.

[104] Eriksson L.-G., Hellsten T. and Willen U., "Comparison of time dependent simulations with experiments in ion cyclotron heated plasmas", Nucl. Fusion **33** (1993) 1037.

[105] Bateman G. et al., "Predicting temperature and density profiles in tokamaks", Phys. Plasmas **5** (1998) 1793.

[106] Ohkawa T., "A transport model for alcator scaling in tokamaks", Phys. Lett. A **67** (1978) 35.

[107] Tubbing B.J.D. et al., "H-mode confinement in JET with enhanced performance by pellet peaked density profiles", Nucl. Fusion **31** (1991) 839.

[108] Zhu P., Bateman G., Kritz A.H. and Horton W., "Predictive transport simulations of internal transport barriers using the Multi-Mode model", Phys. Plasmas **7** (2000) 2898.

[109] Waltz R.E. et al., "A gyro-Landau-fluid transport model", Phys. Plasmas **4** (1997) 2482.

[110] Kinsey J.E., Waltz R.E., Staebler G.M. and St. John H., "Dynamic Modeling of Multi-channel Transport Bifurcations Using Ion Temperature Gradient Based Models for Tokamak Plasmas", Proc. 26th European Physical Society Conf. on Controlled Fusion and Plasma Physics, Maastrict, The Netherlands, 14-18 June, (1999) 1205.

[111] Itoh S.-I. et al., "Self-sustained turbulence and H-mode confinement in toroidal plasmas", Plasma Phys. Control. Fusion **38** (1996) 1743.

[112] Fukuyama A., Takatsuka S., Itoh S.-I., Yagi M. and Itoh K., "Transition to an enhanced internal transport barrier", Plasma Phys. Control. Fusion **40** (1998).

[113] Lopez-Bruna D., Newman D.E., Carreras B.A. and Diamond P.H., "Fluctuation level bursts in a model of internal transport barrier formation", Phys. Plasmas **6** (1999) 854.

[114] Horton W. and Zhu P., "Transport barrier dynamics", Phys. Plasmas **7** (2000) 4534.

[115] Schilham A.M.R., Hogeweij G.M.D., Lopes Cardozo N.J., Parail V.V. and Gormezano C., "Application of the RTP transport model to the JET tokamak", submitted to Nucl. Fusion (2001).

[116] Pereverzev G. et al., "Simulation of ASDEX Upgrade Plasmas with Internal Transport Barrier", Proc. 26th European Physical Society Conf. on Controlled Fusion and Plasma Physics, Maastrict, The Netherlands, 14-18 June, (1999) 1429.

[117] Kotschenreuther M. et al., "Quantitative predictions of tokamak energy confinement from first-principles simulations with kinetic effects", Phys. Plasmas **2** (1995) 2381.

[118] Tala T.J.J. et al. "Impact of Different Preheating Methods on q-profile Evolution in JET", Proc. 28th European Physical Society Conf. on Controlled Fusion and Plasma Physics, Madeira, Portugal, 18-22 June, 2001 541.

[119] Kolesnichenko Ya. et al., *Reviews of Plasma Physics* edited by B.B. Kadomtsev, Plenum, New York, **17** (1992) 1.

[120] Strand P.I. and Houlberg W.A., "Magnetic flux evolution in highly shaped plasmas", Phys. Plasmas **8** (2001) 2782.

[121] Huysmans G.T.A., Hender T.C., Hawkes N.C. and Litaudon X., "MHD stability of Advanced Tokamak Scenarios with reversed central current: An Explanation of the 'Current Hole"', submitted to Phys. Rev. Lett. (2001).

[122] Budny R.V. et al., "Simulations of deuterium-tritium experiments in TFTR", Nucl. Fusion **32** (1992) 429.

[123] Hyusmans G.T.A. et al., "MHD stability analysis of optimised shear discharges in JET", Proc. 24th European Physical Society Conf. on Controlled Fusion and Plasma Physics, Berchtesgaden, Germany, 9–13 June, (1997) **21A** 21.

[124] Tala T.J.J. et al. "Modelling of LHCD Profile Control for High Performance DT Experiments on JET", Proc. 13th Topical Conf. on Radio Frequency Power in Plasmas (AIP Conference Proceedings 485), Annapolis, Maryland, USA, 12-14 April, 1999 207.

[125] Challis C.D. et al., "Influence of the q-profile shape on plasma performance in JET", submitted to Plasma Phys. Control. Fusion in 2002.

[126] Dux R. et al. "Analysis of Impurity Behaviour in ITB Discharges with Reversed Shear on JET", Proc. 28th European Physical Society Conf. on Controlled Fusion and Plasma Physics, Madeira, Portugal, 18-22 June, 2001 505.

Published by

Vuorimiehentie 5, P.O.Box 2000, FIN–02044 VTT, Finland
Phone internat. +358 9 4561
Fax +358 9 456 4374

Series title, number and report code of publication

VTT Publications 467
VTT–PUBS–467

Author(s)
Tala, Tuomas

Title

Transport Barrier and Current Profile Studies on the JET Tokamak

Abstract

One of the crucial problems in fusion research is the understanding of heat and particle transport in plasmas relevant for energy production. The neo-classical theory of tokamak transport is well-established, but it cannot explain experimental results. Instead, the micro-turbulence driven anomalous transport has been found to be dominant in present tokamak experiments.

There are several mechanisms that can locally suppress micro-turbulence and reduce significantly the anomalous transport. These regions of reduced transport are called transport barriers. The presence of Internal Transport Barriers (ITBs) is one of the bases in 'Advanced Tokamak Scenarios'. One of the principal goals in the 'Advanced Tokamak Scenarios' is to improve the fusion power density and confinement with internal transport barriers by controlling the current density profile and maximising the bootstrap current – and ultimately rendering the tokamak compatible with continuous operation.

This thesis reports on studies and modelling of internal transport barriers and current density profiles in the Joint European Torus (JET) tokamak with a fluid transport code. Explanations for the following open questions are sought: what are the mechanisms that govern the formation and dynamics of the ITBs in JET and secondly, how can the current density profile be modified and further, how does it affect ITBs and plasma performance?

On the basis of the empirical study at the ITB transition, the $\omega_{E\times B}$ flow shear and magnetic shear appear as strong candidates in determining the onset time, the radial location and the dynamics of the ITBs in JET. This ITB threshold condition, employed in the semi-empirical Bohm/GyroBohm transport model, has been found to be in good agreement with experimental results in predictive transport simulations. On the other hand, the simulation results from the predictive transport modelling with a theory-based quasi-linear fluid transport model strongly emphasise the importance of the density gradient in the ITB formation.

According to the current density modelling studies, lower hybrid and electron cyclotron current drive are the most versatile current drive methods in terms of the produced q-profile in the preheating phase in JET. With lower hybrid preheating, a core current hole has been found and a physics-based explanation, confirmed by the transport modelling, is given. The predictive transport simulations indicate that application of lower hybrid current drive during the high performance phase can enhance the fusion performance significantly by increasing the ITB radius.

Keywords
nuclear fusion, JET tokamak, plasma transport, heat transport, internal transport barriers, current density, modelling, transport models, flow shear, magnetic shear

Activity unit
VTT Processes, Industrial Physics, Otakaari 3 A, P.O.Box 1404, FIN–02044 VTT, Finland

ISBN			Project number
951–38–5988–6 (soft back ed.) 951–38–5989–4 (URL:http://www.inf.vtt.fi/pdf/)			
Date May 2002	Language English	Pages 71 p. + app. 95 p.	Price D
Name of project		Commissioned by	
Series title and ISSN VTT Publications 1235–0621 (soft back ed.) 1455–0849 (URL: http://www.inf.vtt.fi/pdf/)		Sold by VTT Information Service P.O.Box 2000, FIN–02044 VTT, Finland Phone internat. +358 9 456 4404 Fax +358 9 456 4374	